Lithos 292–293 (2017) 179–197

Contents lists available at ScienceDirect

Lithos

journal homepage: www.elsevier.com/locate/lithos

Slab-derived components in the subcontinental lithospheric mantle beneath Chilean Patagonia: Geochemistry and Sr–Nd–Pb isotopes of mantle xenoliths and host basalt

Tiago Jalowitzki [a,*], Fernanda Gervasoni [b], Rommulo V. Conceição [a], Yuji Orihashi [c], Gustavo W. Bertotto [d], Hirochika Sumino [e], Manuel E. Schilling [f], Keisuke Nagao [g], Diego Morata [h,i], Paul Sylvester [j]

[a] Instituto de Geociências, Universidade Federal do Rio Grande do Sul (UFRGS), Av. Bento Gonçalves, 9500, Prédio 43129, Porto Alegre, RS, Brazil
[b] Faculdade de Ciências e Tecnologia, Universidade Federal de Goiás (UFG), Rua Mucuri, s/n - Setor Conde dos Arcos, Aparecida de Goiânia, GO, Brazil
[c] Earthquake Research Institute, The University of Tokyo, Yayoi 1-1-1, Bunkyo-Ku, 113-0032 Tokyo, Japan
[d] INCITAP, CONICET - Universidad Nacional de La Pampa, Uruguay 151, 6300 Santa Rosa, La Pampa, Argentina
[e] Department of Basic Science, Graduate School of Arts and Sciences, the University of Tokyo, 3-8-1 Komaba, Meguro-ku, Tokyo 153-8902, Japan
[f] Instituto de Ciencias de la Tierra, Facultad de Ciencias, Universidad Austral de Chile, Valdivia 5090000, Región de Los Ríos, Chile
[g] Division of Polar Earth-System Sciences KOPRI (Korea Polar Research Institute), 26 Songdomirae-ro, Yeonsu-gu, Incheon 21990, Republic of Korea
[h] Departamento de Geología, Facultad de Ciencas Físicas y Matemáticas, Universidad de Chile, Plaza Ercilla 803, Santiago, Chile
[i] Centro de Excelencia en Geotermia de los Andes (CEGA), Fondap-Conicyt, Chile
[j] Department of Geosciences, Texas Tech University, 125 Science Building, Lubbock, TX 79409-1053, USA

ARTICLE INFO

Article history:
Received 30 November 2015
Accepted 7 September 2017
Available online 14 September 2017

Keywords:
Coyhaique spinel-peridotites
Slab-derived metasomatism
HIMU-like host basalt
Andean back-arc
Chilean Patagonia

ABSTRACT

In subduction zones, ultramafic xenoliths hosted in alkaline basalts can yield significant information about the role of potential slab-derived components in the subcontinental lithospheric mantle (SCLM). Chemical and isotopic heterogeneities in such xenoliths are usually interpreted to reflect melt extraction followed by metasomatic re-enrichment. Here we report new whole-rock major, trace element and isotopic (Sr–Nd–Pb) data for a Proterozoic suite of 17 anhydrous spinel-lherzolites and Eocene (new K–Ar data) host alkaline basalt found near Coyhaique (~46°S), Aysén Region, Chile. These Patagonian nodules are located in a current back-arc position, ~100 km east of the present day volcanic arc and ~320 km from the Chile Trench.

The mantle xenoliths consist of coarse- to medium-grained spinel-lherzolites with trace element compositions characteristic of a subduction zone setting, such as pronounced negative Nb, Ta and Ti anomalies coupled with significant enrichment of LILEs (e.g., U) and chalcophile elements (W, Pb and Sn). Most of them are characterized by flat to depleted light-rare earth element (LREE) patterns ($Ce/Yb_N = 0.6–1.1$) coupled with less radiogenic Sr–Pb ($^{87}Sr/^{86}Sr = 0.702422–0.703479$; $^{206}Pb/^{204}Pb = 18.212–18.539$) and more radiogenic Nd isotopic compositions ($^{143}Nd/^{144}Nd = 0.512994–0.513242$), similar to the depleted mantle component (DMM or PREMA). In contrast, samples with slight LREE enrichment ($Ce/Yb_N = 1.3–1.8$) show more radiogenic Sr–Pb ($^{87}Sr/^{86}Sr = 0.703791–0.704239$; $^{206}Pb/^{204}Pb = 18.572–18.703$) and less radiogenic Nd isotopic compositions ($^{143}Nd/^{144}Nd = 0.512859–0.512934$), similar to the EM-2 reservoir. These new geochemical and isotope data suggest that the Coyhaique spinel-lherzolites are derived from a heterogeneous SCLM resulting from mixing between a depleted mantle component and up to 10% of slab-derived components. The enriched component added to the SCLM represents variable extents of melts of both subducted Chile Trench sediments and modified oceanic crust throughout the initial stages of the Farallón–Aluk ridge collision during Paleocene to Eocene time. However, based on the tectonic evolution of southern South America, we cannot exclude the influence of long-lived subduction events beneath south Patagonia. Although we believe that the studied samples were brought to the surface in this geodynamic context, there is no evidence that ocean island basalt (OIB)–like melts related to the Farallón–Aluk asthenospheric slab window affected the peridotite composition.

The host alkaline basalt is a single unit with a HIMU-like OIB signature characterized by marked positive Nb–Ta anomalies coupled with negative anomalies in highly incompatible and fluid-mobile elements (Rb, K, Pb, and Sr). The compositional similarity between the HIMU-like OIB mantle source and the host basalt is also evident from trace element ratios [(Ba–Th–K–La–Zr)/Nb] as well as by the low $^{87}Sr/^{86}Sr_i$ (0.703039–0.703058) and relatively high $^{143}Nd/^{144}Nd_i$ (0.512880–0.512874) and $^{206}Pb/^{204}Pb$ (19.333–19.389) isotopic ratios. The low $^{206}Pb/^{204}Pb$ ratios compared to end-member HIMU lavas (e.g., Sta. Helena and the Cook-Austral Islands) suggest that this

* Corresponding author at: Instituto de Geociências, Universidade Federal do Rio Grande do Sul (UFRGS), Av. Bento Gonçalves, 9500 - Prédio 43129, Bairro Agronomia, Porto Alegre, RS CEP: 91501970, Brazil.
E-mail address: tiago.jalowitzki@ufrgs.br (T. Jalowitzki).

https://doi.org/10.1016/j.lithos.2017.09.008

region was modified by processes associated with a prolonged period of subduction related to the Andean orogenesis and the recycling of several oceanic plates beneath the continent, following the Mesozoic breakup of Gondwana or an even older subduction-related event with young recycling ages (<2 Ga).

1. Introduction

Patagonian mantle xenoliths represent samples of the subcontinental lithospheric mantle (SCLM) in an active subduction zone setting and are typically carried to the surface by alkaline magmatism in the Andean back-arc region. The geochemical and isotopic characteristics of the mantle xenoliths and their host lavas, particularly those located close to the margin of the convergent plates, can provide valuable information about heterogeneities in the SCLM at the latitudes of the Southern and Austral Volcanic Zones (e.g., Bjerg et al., 2009; Faccini et al., 2013; Gervasoni et al., 2012; Gorring and Kay, 2000; Jalowitzki et al., 2010, 2016; Kilian and Stern, 2002; Mundl et al., 2015; Ntaflos et al., 2007; Rieck et al., 2007; Rivalenti et al., 2004; Schilling et al., 2005, 2017; Stern et al., 1999). Mantle xenoliths are often lithologically and geochemically heterogeneous, even within xenoliths from the same volcano (Bjerg et al., 2009). Thus, the nature and evolution of different mantle domains, and the influence of subduction versus asthenospheric materials on the SCLM are a topic of continuing debate and therefore a fruitful area of research.

In southern South America, the Andean volcanic arc is related to the convergent boundary between the South American plate and both the Nazca and Antarctic plates. The Andean convergent margin allows a (re)-fertilization of the SCLM by the subducting slab, which may provide 1) pelagic and terrigenous trench sediments, 2) slab-derived water-rich fluids, 3) altered oceanic lithosphere (e.g., gabbros, basalts, peridotites, and serpentinites), 4) adakitic melts generated by partial melting of the subducted oceanic crust, 5) delamination and tectonic erosion of the lower crust, and 6) asthenospheric upwelling through slab windows produced by subduction of spreading ridges. Previous studies of plate tectonic reconstructions documented subduction of at least two active spreading ridges beneath the western margin of southern South America at the latitude of the Taitao Peninsula during the Cenozoic: the Farallón–Aluk (Phoenix) ridge and the current Chile spreading ridge (e.g., Breitsprecher and Thorkelson, 2009; Cande and Leslie, 1986). Subductions of these spreading-ridges since the early Eocene (~54 Ma) were responsible for both modern and ancient Patagonian slab windows.

To better understand the heterogeneities and tectonic evolution of the SCLM of South Patagonia, we studied the petrography, whole-rock major and trace elements, and the Sr–Nd–Pb isotopic compositions of 17 Proterozoic (1.3–1.7 Ga; Schilling et al., 2017) anhydrous spinel-peridotites and the Eocene (~54 Ma; new K–Ar age) host basalt located ~100 km east of the present-day volcanic arc, in the Aysén Region of Chilean Patagonia. Based on these new data, we discuss the influence of slab-derived components on the composition of the SCLM and the possible relationship of the host basalt with the Paleocene–Eocene slab window formed by the subduction of the Farallón–Aluk spreading ridge beneath the South American plate.

2. Geological setting and samples

Although the Paleozoic to Mesozoic reconstruction of southwestern margin of Gondwana records subduction events in south Patagonia, the oldest events are not well constrained due to pervasive overprinting by Permo-Triassic and younger episodes (e.g., Cawood and Buchan, 2007). Since the Middle Jurassic, persistent igneous activity of calc-alkaline affinity, ranging from basaltic andesites to rhyolitic tuffs and ignimbrites, as well as cogenetic plutonic rocks belonging to the Patagonian batholith, are associated with the subduction zone formed around 46°S (Baker et al., 1981; Hervé et al., 2007; Pankhurst et al., 1999). The Patagonian batholith is comprised of the North Patagonian batholith (NPB, north of 47°S), the South Patagonian batholith (SPB, 47–53°S), and the Fuegian batholith (south of 53°S) (Hervé et al., 2007).

The Aysén Region (44–47°S) is characterized by the presence of the NPB, a large and widely distributed calc-alkaline plutonic complex that developed as a result of eastward subduction of the Nazca plate (~200 km; Demant et al., 1996, Hervé et al., 2007; Pankhurst et al., 1999). To the west, this batholith intrudes Chonos Late Paleozoic metamorphic complex while to the east it intrudes Paleozoic and Mesozoic volcanic and sedimentary units (Demant et al., 1996 and references therein; Pankhurst et al., 1999).

Currently, the Patagonian western margin is recording the continuous subduction of the Chile Ridge spreading centre, which intersects the Chile Trench at the latitude of the Taitao Peninsula and forms a trench-ridge-trench triple junction (Cande and Leslie, 1986) (Fig. 1). The collision of the Farallón and Aluk oceanic plates against the South America continental plate generated the Farallón–Aluk–South America triple junction, which migrated southward along the South American trench from Paleocene to Eocene time (Espinoza et al., 2005; Morata et al., 2000; Parada et al., 2001; Ramos and Kay, 1992). This process allowed the opening of the first documented slab window beneath the Patagonian province, as recorded by the alkaline Eocene plateau basalts of Central Patagonia.

The Cenozoic Patagonian continental back-arc province (34°–54°S) is characterized by a widely distributed and voluminous tholeiitic main-plateau magmatism followed by less-voluminous, post-plateau magmatism. The main-plateau lavas form large and elevated plateaus, such as Somún Curá, del Lago Buenos Aires, de la Muerte, Belgrano, and Central. Mantle xenoliths occasionally occur in the main-plateau lavas. Post-plateau magmas mainly consist of alkaline basaltic lava flows and monogenetic cinder cones with an OIB-like signature and often host mantle xenoliths. In the Chilean back-arc domain, the Aysén plateau basalts (ca. 46°S) occur north of the General Carrera Lake and are close to the international border between Chile and Argentina (Fig. 1a). The Cenozoic volcanism in this region is composed of a Paleocene–Eocene (60–46 Ma) sequence of olivine-phyric flood basalts covered by Miocene to Pliocene continental sediments with intercalated acidic pyroclastic units (Baker et al., 1981; Butler et al., 1991; Demant et al., 1996; Morata et al., 2000; Parada et al., 2001).

The Coyhaique lava flow containing mantle xenoliths has a thickness of ~4 m and is part of a subhorizontal sequence of basalts exposed to the northwest of the Balmaceda locality (known as Balmaceda Basalts), which reaches a maximum thickness of ~150 m. These mantle xenoliths and the host lava, initially described by Morata et al. (2000), are located approximately 30 km SE from the city of Coyhaique, ~100 km east of the modern volcanic arc, and ~320 km from the Chile Trench. This locality is particularly close to the Macá, Cay and Hudson volcanoes (Fig. 1a). The Coyhaique mantle xenoliths are among the closest to the margin of the convergent plates, together with Cerro del Fraile and Chile Chico, which are located 280 to 300 km from the Chile Trench, respectively.

The most plausible tectono-magmatic evolution that has been proposed to explain the Eocene back-arc magmatism in this region involves asthenosphere upwelling in response to the opening of the Patagonian slab window, which was a consequence of Farallón–Aluk

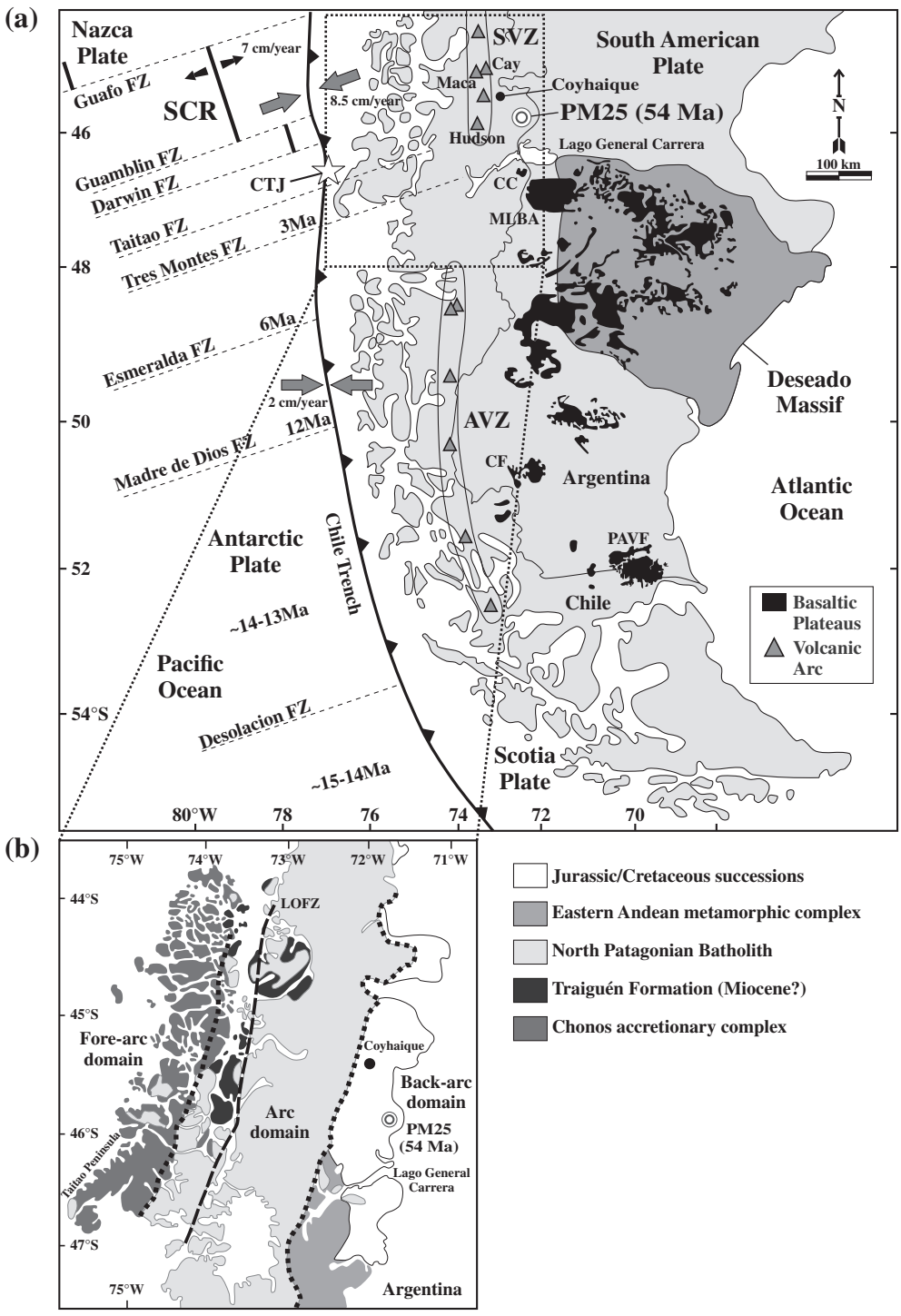

Fig. 1. (a) Present-day tectonic setting of southern South America, modified from Boutonnet et al. (2010). SVZ = Southern Volcanic Zone, AVZ = Austral Volcanic Zone, CTJ = Chile Triple Junction, CC = Meseta de Chile Chico, MLBA = Meseta del Lago Buenos Aires, CF = Cerro del Fraile, and PAVF = Pali-Aike Volcanic Field. (b) Simplified geological map of the Patagonian Cordillera between 43°30′S and 47°30′S showing the main geological units (modified from Pankhurst et al., 1999). LOFZ = Liquiñe-Ofqui Fault Zone. The white circles indicate the location of the studied samples.

ridge subduction (Demant et al., 1996; Morata et al., 2000; Ramos and Kay, 1992). The host basaltic rock and 17 mantle xenoliths studied here were collected from the Balmaceda Basalt unit (45°46′S; 71°47′W; PM: Projeto Manto: scientific project led by the Universidade Federal do Rio Grande do Sul, Brazil) (Fig. 1) and were selected to be representative of the larger collection. The studied mantle xenoliths are up to 11 cm in diameter and are fresh, with only a few xenoliths (samples PM25-18 and PM25-38) exhibiting oxidized iron surfaces in hand specimens.

3. Analytical techniques

3.1. Major and trace elements

3.1.1. Host basalt

The whole-rock geochemistry of two samples of the host basalt was determined using the geo-analytical facilities of the Earthquake Research Institute at the University of Tokyo. Major and selected trace element abundances (Sc, V, Cr, Co, Ni, Zn, Ga, Rb, Sr, Y, Zr, Nb and Ba)

were analysed using X-ray fluorescence (XRF, PW2400; Philips Japan Ltd.). The abundances of other trace elements (Cs, Ta, Hf, Pb, Th, U, and rare earth elements - REE) were obtained using an inductively-coupled plasma mass spectrometer (ICP-MS Plasma Quad 3; VG Scienta Holdings AB) connected to a frequency-quadrupled 213 nm Nd: YAG laser ablation (LA) system (UP-213; New Wave Research Inc.). Both sets of data were obtained using the same glass beads, which were prepared by first mixing 1.8 g of rock powder with 3.6 g of lithium metaborate/tetraborate flux. Then, 0.54 g of lithium nitrate was added to the sample powder as an oxidizer, and both were mixed in a torch-mixer for 3 min. The mixture was heated to 1200 °C for 15 min in a 95%Pt–5%Au crucible (30-mm inner diameter) in an automatic bead sampler. Details of the analytical procedures of the XRF and LA-ICP-MS methods are described in Tani et al. (2002) and Orihashi and Hirata (2003), respectively.

3.1.2. Mantle xenoliths

Whole-rock analyses were performed at the Earth Resources Research and Analysis (TERRA) facility, Department of Earth Sciences, Memorial University of Newfoundland, Canada. Major and trace element abundances were obtained using X-ray fluorescence (Bruker S8 Tiger sequential wavelength-dispersive XRF) and ICP-MS (PerkinElmer ELAN DRCII), respectively. The XRF data were obtained using glass beads, which were prepared by mixing 1.5 mg of rock powder with 6.0 mg of lithium metaborate and 1.5 mg of lithium tetraborate. The mixture was placed into a platinum crucible, and five drops of lithium bromide were added as a wetting agent. The crucibles were then placed in the Leco Fluxer and heated at ~850 °C for 8.5 min and fused at ~1050 °C for 11.5 min. For each run of 20 samples, six reference materials (JB-1A-G, MRG-1-G, SY-2-G, SY-3-G, SIO2-G, BIR-1-G) were run four times each, as calibration standards.

The ICP-MS data were obtained from rock solutions, where 0.1 g of sample powder was digested using the high-pressure digestion technique developed by Diegor et al. (2001). The method consists of three cycles of acid attacks: the first was performed with HF-HNO_3 in a conventional oven at 200 °C; the other two cycles were made only with HNO_3 on a hotplate at 70 °C. After the acid fractions, the samples were dried completely. For the final solutions, 1.35 ml of oxalic acid was added to each sample to complex Fe and other trace elements, and 0.665 ml of HF-boric acid mixture (0.1 M HF/0.45 M boric acid) was added to stabilize Nb and Ta, and to complex excess free F^- ions.

The samples were analysed in two routines: the "trace package", which measured the isotopes: ^{85}Rb, ^{86}Sr, ^{89}Y, ^{90}Zr, ^{93}Nb, ^{133}Cs, ^{137}Ba, ^{139}La, ^{140}Ce, ^{141}Pr, ^{145}Nd, ^{147}Sm, ^{151}Eu, ^{160}Gd, ^{159}Tb, ^{163}Dy, ^{165}Ho, ^{167}Er, ^{169}Tm, ^{173}Yb, ^{175}Lu, ^{177}Hf, ^{181}Ta, ^{206}Pb, ^{207}Pb, ^{208}Pb, ^{232}Th, ^{238}U, and the "environmental/exploration package" which measured the isotopes ^{49}Ti, ^{118}Sn and ^{183}W. Both methods employ a combination of external calibration, surrogate calibration, standard addition, and an internal standard for data reduction, which deal with interrelated matrix, drift, and interference issues (Jenner et al., 1990). The internal calibration standard added to the samples analysed with the "trace package" method was composed of Li, Sr, Zr, Cs, Ba, La, Pr, Nd, Sm, Er, Tm, Tl, Bi, and U. Another internal standard solution of In was added to each sample with the peristaltic pump, during each of the analyses in a run. The internal calibration standard added to the samples analysed in the "environmental/exploration package" was composed of Sc, In, Re, and U.

The detailed description of the "trace package" method was presented by Jenner et al. (1990) and the description of the "environmental/exploration package" was reported by Diegor et al. (2001). The analyses were performed with a total counting time per mass of 10 s at one point per peak, and dwell time per mass of 0.05 s. To monitor the quality of the analysis, the reference material MRG-1-F1 was analysed and one sample was duplicated (Table A.1). Data were reduced first by a background-correction, using the analysis of the blank and the solutions with and without the internal standard. Drift was corrected using the signal from the In internal standard and the matrix corrections were performed with the external calibrations.

3.2. Sr–Nd–Pb isotopes

Sr–Nd–Pb isotopic ratios for 15 mantle xenoliths and two basaltic rocks were measured at the Laboratório de Geologia Isotópica, Universidade Federal do Rio Grande do Sul (UFRGS), Porto Alegre, Brazil. The samples were leached with cold 0.25 N HCl in an ultrasonic bath for 30 min to remove impurities. When dried, 0.1 g of each mantle xenolith sample was spiked with a mixed $^{87}Rb/^{84}Sr$ and $^{149}Sm/^{150}Nd$ tracer. The host basalt samples were not spiked. Dissolution procedures were performed with HF, HNO_3 and HCl in Teflon vials (Savillex®), which were warmed on a hot plate until samples were completely dissolved. In the next stage, the sample solutions were diluted in 3 ml of 2.5 N HCl and stored in test tubes. An aliquot of 1 ml of each sample solution was used to separate the Rb, Sr and REE by AG-50 W-X8 (200–400 mesh) cation exchange columns, followed by Sm and Nd separation using anionic LN-B50-A (100–150 mesh) resin. The Pb was separated using anionic BioRad-AG1X (200–400 mesh) resin in an HBr solution. Individual solutions of Rb, Sr, Sm, Nd and Pb were dried in Teflon vials (Savillex®) on a hot plate. The residues were deposited onto single Ta (for Rb, Sr, Sm and Pb) and triple Ta–Re–Ta (for Nd) filaments.

Mass spectrometric analyses of the radiogenic isotopes were performed using two different thermal ionization mass spectrometers (Sector 54, VG Scienta Holdings AB; and Triton, Thermo Scientific). The data were corrected for mass fractionation by normalizing to $^{86}Sr/^{88}Sr = 0.1194$ and $^{146}Nd/^{144}Nd = 0.7219$. The replicate analyses of NBS-987 and JNd-1 standards gave $^{87}Sr/^{86}Sr = 0.710254 \pm 19$ ($n = 4$, 2σ) and $^{143}Nd/^{144}Nd = 0.512101 \pm 8$ ($n = 4$, 2σ). For Pb NBS-981, the variation from the accepted values was less than 0.01%/a.m.u.

3.3. K–Ar ages

The new K–Ar ages for the two basaltic rocks were analysed using the unspiked sensitivity method. The Ar analyses were performed using a noble gas mass spectrometry system (MS-III) at the Geochemical Research Center, Graduate School of Science, University of Tokyo. The whole-rock samples (0.3–0.6 g) were crushed and sieved using a 60–80 mesh, wrapped in 10 μm thick aluminium foil and loaded into a glass sample holder, which was connected to an extraction oven. The samples were fused at 1700 °C in a vacuum in the oven. Evaporated gas for Ar purification was introduced directly using a vacuum line. The Ar isotope analyses were performed using a modified VG-5400 mass spectrometer on a small amount of Ar gas ($<2 \times 10^{-7}$ cm^3 STP). When the amount of Ar gas extracted from the sample exceeded this limit, it was reduced using a known volume of the purification line. The errors in the ^{40}Ar sensitivity and $^{40}Ar/^{36}Ar$ ratio are estimated to be 5% and 0.2%, respectively, based on repeated measurements of the atmospheric standard gas, which contained 1.5×10^{-7} cm^3 STP of ^{40}Ar. The errors in the $^{40}Ar/^{36}Ar$ ratios were deduced from the statistical 1σ errors for the samples, standard gases and blank correction. The K concentration for the aliquot of the rock fractions used for the Ar analysis was determined using X-ray fluorescence (XRF, PW2400; Philips Japan Ltd.) at the Earthquake Research Institute, University of Tokyo. The details of the procedures are described in Nagao et al. (1991) and Orihashi et al. (2004).

4. Results

4.1. Mantle xenoliths

4.1.1. Petrography

An optical petrographic microscope was used to identify textures and mineral constituents of the studied mantle xenoliths. A scanning

electron microscope (JSM-6610LV SEM) with energy dispersive system (EDS) microanalysis was used to determine semi-quantitative mineral compositions.

The modal proportions of the minerals (Table A.2) were determined by point-counting, using 900–2800 points that covered the entire area of each relatively large thin section (2.5 × 4.5 cm). The Coyhaique peridotites are classified as anhydrous spinel-lherzolites (Fig. 2a). They are composed of olivine (42–63 vol.%), orthopyroxene (16–39 vol.%), clinopyroxene (10–20 vol.%) and spinel (2–4 vol.%) (Figs. 2b, 3a, b and 4a, b). Olivine and orthopyroxene are the dominant minerals, with subordinate clinopyroxene and accessory spinel (chromium–aluminium spinel). In thin section, the alteration has been developed mainly in olivine, which has been partially transformed to red-brown to yellow iddingsite in grain rims and fractures (Figs. 3c, d and 4d). As shown in Table A.3, iddingsite formation involves the addition of Fe_2O_3 and SiO_2 and the removal of MgO. The representative chemical compositions of the mineral phases shown in Table A.3 are similar to those reported by Morata et al. (2000) and Schilling et al. (2017).

Coarse- to medium-grained spinel-lherzolites (grain sizes ranging from ~1 to ~17 mm) have a protogranular to porphyroblastic microtexture (Mercier and Nicolas, 1975), as evidenced by large orthopyroxene porphyroblasts with lobate grain boundaries and smaller grains (neoblasts) (Fig. 2b). There is no obvious preferred crystal orientation or strain-induced elongation, as well as whole mineral recrystallization (equigranular texture). These textural characteristics imply a SCLM with low strain and recrystallization rates resulting from the deformation of the primary protogranular rock. Representative thin section photomicrographs of the studied samples are presented in Fig. 3. The shapes of the olivine porphyroblasts (up to 8 mm in diameter) range from subhedral to anhedral, with straight to gently curved grain boundaries, commonly fractured and often exhibiting undulatory extinction and kink bands (Fig. 3c, d). Orthopyroxene porphyroblasts (up to 17 mm in diameter) have irregular shapes with curvilinear boundaries, evolving locally to polygonal arrangements with 120° triple junctions. The largest orthopyroxene grains contain numerous thin exsolution lamellae of clinopyroxenes and sometimes they display kinks (Figs. 3e, f and 4e). Clinopyroxene are Cr-rich diopside (Cr_2O_3 > 1.0 wt.%) and occur as dark green crystals (up to 5 mm in diameter), which sometimes present spongy rims that are poor in Na_2O and Al_2O_3 but rich in CaO and MgO (Fig. 4f and Table A.3). Spinel is usually black, but in some cases shows a brown colour. They are interstitial, typically with a holly-leaf shape (Fig. 3a, b), and also occur as inclusions, usually in pyroxenes.

4.1.2. Whole-rock geochemistry

The whole-rock major and trace element compositions and loss on ignition (LOI) data of the 17 Coyhaique spinel-lherzolites are presented in Table 1. Fig. 5 presents selected major element variation diagrams with each oxide plotted against MgO wt.%. Published data for whole-rock anhydrous spinel-peridotites from Patagonia are also plotted (Fig. 5; see details in the figure caption). Most spinel-lherzolites show relatively low SiO_2 (<44.5 wt.%) and similar to high MgO (>38.0 wt.%) when compared to primitive mantle (PM - McDonough and Sun, 1995; SiO_2 = 44.9 wt.% and MgO = 37.7 wt.%) and depleted MORB mantle (DMM - Workman and Hart, 2005; SiO_2 = 44.7 wt.% and MgO = 38.7 wt.%). The main oxides (SiO_2, TiO_2, Al_2O_3, CaO, and Na_2O) show negative correlations with MgO (Fig. 5), which are usually attributed to different degrees of partial melting of the same fertile source. The other major and compatible trace elements (e.g., Cr, Co, Zn) exhibit scattered correlation (not shown). In our samples, Ni is positively correlated with MgO (r^2 = 0.87), which is consistent with its compatible character during melt-peridotite equilibrium (Fig. 5f). Mg-numbers range from 88.6 to 90.1 and overlaps that of typical residual peridotites, but values lower than 89 (n = 5) indicate that some of the peridotites are more fertile than canonical primitive mantle (e.g., McDonough and Sun, 1995). The high contents of CaO (2.4–3.3 wt.%) and Al_2O_3 (2.7–3.9 wt.%) observed in our samples indicate a fertile and possibly metasomatized composition, which are consistent with the high modal percent of both clinopyroxene and spinel, respectively. Compared with other whole-rock xenolith suites of anhydrous spinel-peridotites from Patagonia, the studied mantle samples from Coyhaique have relatively lower MgO coupled with higher TiO_2, Al_2O_3, CaO, and Na_2O contents (Fig. 5a–e). Contrary, samples from Agua Poca volcano, located in the central-western of Argentina, show higher TiO_2 and similar MgO, Al_2O_3, CaO, and Na_2O than Coyhaique spinel-peridotites (Jalowitzki et al., 2010; Fig. 5a–e).

In general, on the PM (primitive mantle)-normalized multi-element diagram (Sun and McDonough, 1989; Fig. 6a, b), the spinel-lherzolites studied here show negative Nb, Ta and Ti anomalies coupled with a significant enrichment in large ion lithophile elements (LILE; e.g., U) and in the chalcophile elements (W, Pb and Sn). Inversely, Cs, Rb, Ba and Sr do not show a well-defined pattern and vary from slightly negative to positive anomalies. In the PM-normalized rare earth element (REE) diagram (Fig. 6c), the majority of the spinel-lherzolites show flat patterns (Ce/Yb_N = 0.92–1.07), whereas some of them show a slight light-REE (LREE) depletion (Ce/Yb_N = 0.61–0.64) to LREE-enrichment

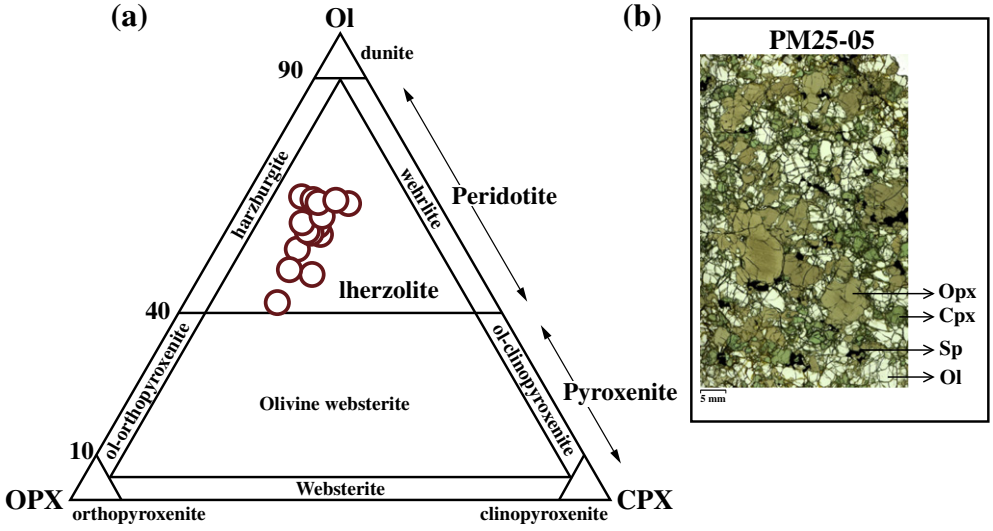

Fig. 2. (a) Mineral proportions (wt.%) of the Coyhaique mantle xenoliths plotted on the ternary classification diagram of Streckeisen (1979). (b) Petrographic characteristics of a representative coarse-grained, protogranular to porphyroblastic Coyhaique spinel-lherzolite (PM25-05). Abbreviations: Ol = olivine; Opx = orthopyroxene; Cpx = clinopyroxene; Sp = spinel.

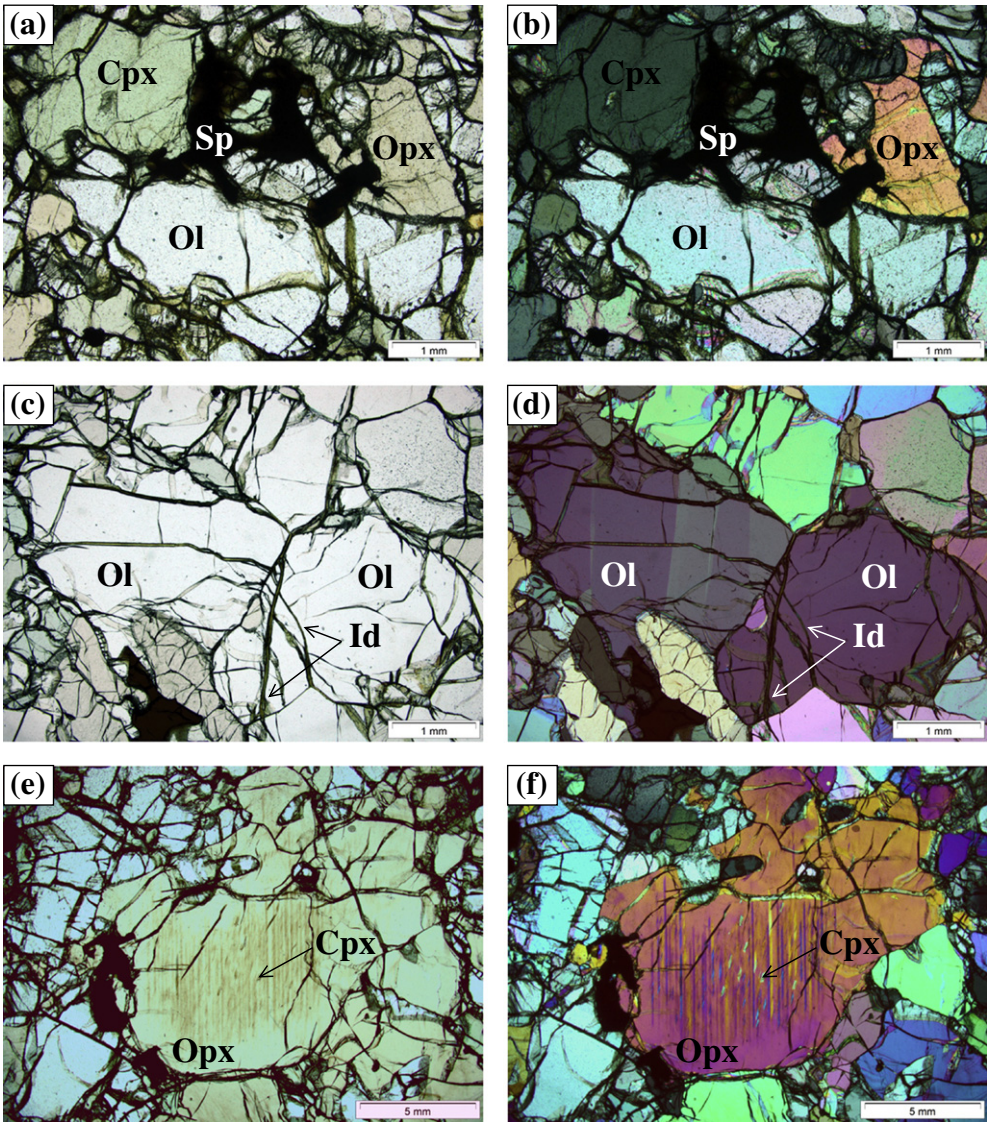

Fig. 3. Photomicrograph showing different textures observed in the Coyhaique lherzolites. The photographs show both plane- and crossed-polarized light in thin sections: (a–b) Interstitial spinel and its typical holly-leaf texture; (c–d) fractured olivine with undulatory extinction (and kink bands) and occurrence of iddingsite (Id); (e–f) orthopyroxene porphyroblast containing thin exsolution lamellae of clinopyroxene, especially in their central parts.

(Ce/Yb_N = 1.25–1.79). The heavy-REE (HREE) abundances of most of the Coyhaique spinel-lherzolites are similar to those of primitive mantle composition and slight higher than DMM.

The compositions of Coyhaique host basalt, DMM (Workman and Hart, 2005), Chile Trench sediments average (Jacques et al., 2013; Kilian and Behrmann, 2003; Lucassen et al., 2010; Shinjoe et al., 2013), Chile Ridge modified oceanic crust (Karsten et al., 1996), OIB and enriched MORB averages (OIB and E-MORB; Sun and McDonough, 1989) are plotted for comparative purposes in both multi-element and REE diagrams (Fig. 6a, c).

The spinel-lherzolites studied here have Nb/Ta (5.18–15.71; commonly < 10) and Nb/La (0.06–0.42) ratios lower than the average of CI chondrites (Sun and McDonough, 1989; Nb/Ta = 17.6; Nb/La = 1.04), which attests to the depleted signature of the SCLM beneath the Coyhaique locality. However, the positive anomalies of the chalcophile elements coupled with Ce/Pb (commonly < 15) and Nb/U (<5) ratios significantly lower than the PM and DMM values (Ce/Pb = 25 and 31; Nb/U = 34 and 46, respectively), as well as strong negative Nb anomalies [$Nb/Nb^* = 0.05–0.35$, where $Nb/Nb^* = Nb_N/(Th_N * La_N)^{1/2}$], indicate that variable fractions of a subduction-related component were involved in the genesis of the spinel-lherzolites.

The Sr–Nd–Pb isotopic data of spinel-lherzolites are given in Table 2. The La/Sm ratios are negatively correlated with Nd isotopic ratios and positively correlated with Pb and Sr isotopic ratios (Fig. 7) (see details about isotope ratios below). The Sr–Nd–Pb isotopes together with La/Sm ratios for all studied spinel-peridotites show good linear correlations (r^2 = 0.82–0.86) between the depleted mantle and a slab-derived melt (50% Chile Trench sediments + 50% modified oceanic crust; Fig. 7). Additionally, Pb/Ce, (Ce–Th)/Yb, and Sr/Th ratios corroborate with this approach.

Diagrams showing relationships between Sr–Nd–Pb isotopes for the spinel-lherzolites are presented in Fig. 8. Also plotted for comparison are other previously published Patagonian whole-rock anhydrous spinel-peridotites (Jalowitzki et al., 2016; Mundl et al., 2015; Ntaflos et al., 2007; Schilling et al., 2005; Stern et al., 1999), Chile Ridge mid-ocean ridge basalts (Bach et al., 1996; Karsten et al., 1996; Sturm et al., 1999), Chile Trench sediments (CTS; Jacques et al., 2013; Lucassen et al., 2010), altered oceanic crust (AOC; Hauff et al., 2003), modified oceanic crust (MOC; Karsten et al., 1996), Andean volcanic arc basalts (Hickey et al., 1986; Hickey-Vargas et al., 1989), and HIMU-like basalts from Pali-Aike Volcanic Field (Choo et al., 2012; D'Orazio et al., 2000; Stern et al., 1990) and Antarctic Peninsula (Hole, 1990; Hole et al.,

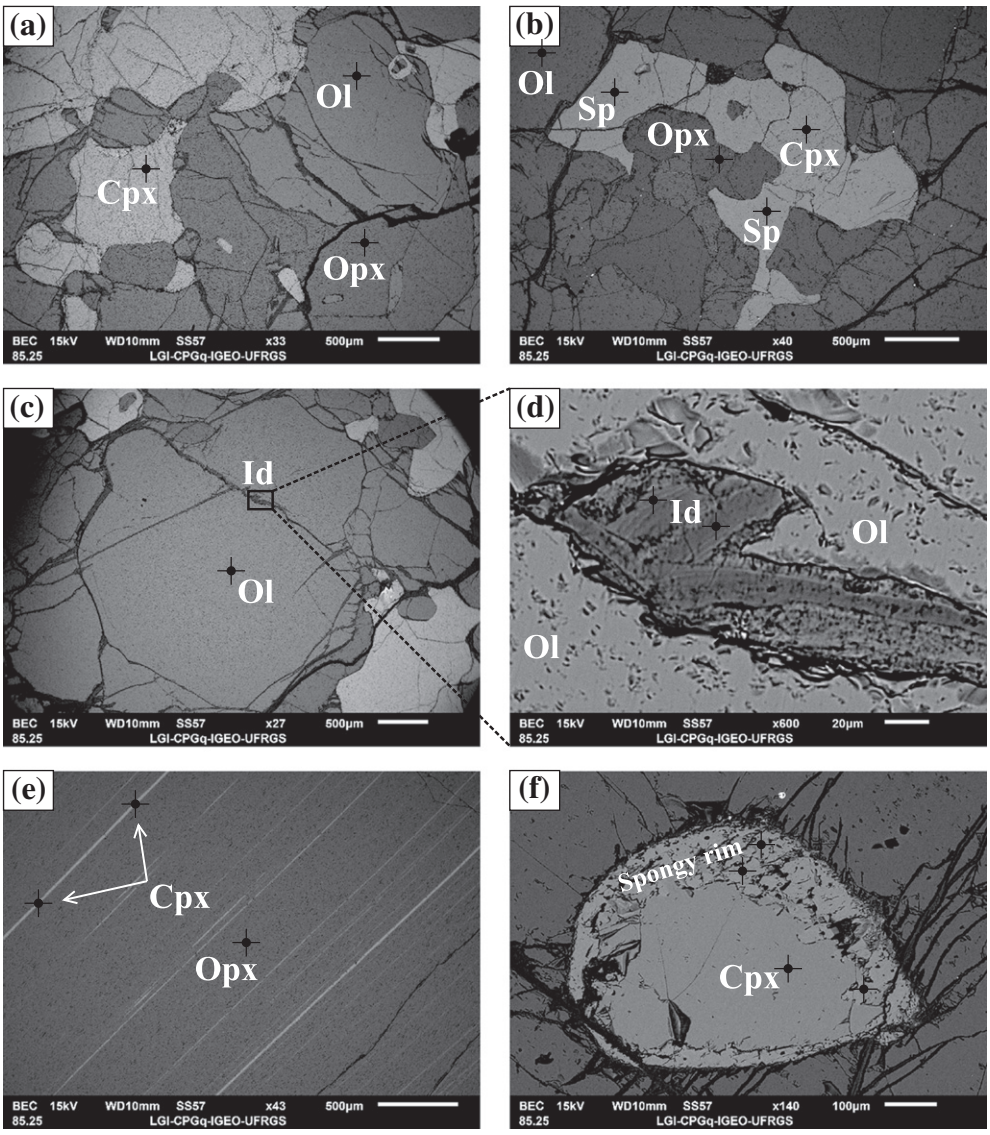

Fig. 4. Scanning electron microscope, backscattered electron (BSE) images of the Coyhaique lherzolites. (a) Coarse- to medium-grained lherzolite with protogranular to porphyroblastic textures evidenced by large olivine and orthopyroxene porphyroblasts with lobate grain boundaries; (b) Coarse- to medium-grained lherzolite with spinel holly-leaf; (c) olivine porphyroblast containing an iddingsite vein; (d) detail of the iddingsite vein; (e) clinopyroxene exsolution lamellae in an orthopyroxene porphyroblast; (f) spongy reaction rim in clinopyroxene.

1993). The following mantle reservoir end-member compositions are also plotted: DMM (Workman and Hart, 2005), HIMU (Hanyu et al., 2014), Enriched Mantle-1 (EM-1; Salters and Sachi-Kocher, 2010), Enriched Mantle-2 (EM-2; Workman et al., 2004), and Prevalent Mantle (PREMA; Wörner et al., 1986).

The Coyhaique spinel-lherzolites have $^{87}Sr/^{86}Sr$ ratios ranging from 0.702422 to 0.704239 and $^{143}Nd/^{144}Nd$ ratios ranging from 0.512859 to 0.513242 ($\varepsilon Nd = +4.3$ to $+11.8$). The Pb isotope ratios vary over the ranges of $^{206}Pb/^{204}Pb = 18.212–18.703$, $^{207}Pb/^{204}Pb = 15.483–15.590$, and $^{208}Pb/^{204}Pb = 37.914–38.524$ (Table 2). The combined Sr–Nd–Pb isotopic signatures of these peridotites show a large range, indicating a significant heterogeneity in the SCLM beneath the Coyhaique locality (Fig. 8). Samples with less radiogenic Sr–Pb and more radiogenic Nd isotopic compositions, which are similar to the depleted mantle component (DMM or PREMA), have flat- to LREE-depleted PM-normalized REE patterns. The variation in the Sr–Nd–Pb isotopic compositions of the less enriched spinel-lherzolites overlap with those obtained from the Chile Ridge basalts. In contrast, samples with more radiogenic Sr-Pb and less radiogenic Nd isotopic compositions show slight LREE enrichment, similar to the EM-2 reservoir. Furthermore, the Sr–Nd–Pb isotope data of enriched samples overlap the values of Chile Trench sediments and Andean volcanic arc basalts (Fig. 8). All Coyhaique peridotites show well-defined linear trends ($r^2 = 0.90–0.97$) between the depleted mantle and the slab-derived melt (50% Chile Trench sediments +50% modified oceanic crust) on plots of Sr–Nd–Pb isotopes (Fig. 8).

In comparison with xenoliths from other Patagonian localities, our samples show a similar range of Sr and Nd isotope values to some mantle samples from Gobernador Gregores (Jalowitzki et al., 2016; Mundl et al., 2015), Pali-Aike Volcanic Field (Jalowitzki et al., 2016; Mundl et al., 2015; Stern et al., 1999), and Tres Lagos (Mundl et al., 2015; Ntaflos et al., 2007) (Fig. 8a). However, the data from Tres Lagos reported by Ntaflos et al. (2007), as well as the spinel-lherzolites from Cerro Redondo (Schilling et al., 2005) have enriched isotope signatures, suggesting a strong contribution of the EM-2 component (Fig. 8a). As exceptions, three samples from Tres Lagos and one from Cerro Redondo show decoupling of the Sr–Nd system (Fig. 8a), where Sr isotopic ratios increase at constant Nd isotopic composition, likely due to the host basalt infiltration or to the chromatographic processes (Ntaflos et al., 2007; Schilling et al., 2005). Pb isotopic data of whole-rock anhydrous

Table 1
Whole-rock major and trace element compositions for the Coyhaique mantle xenoliths determined by XRF and ICP-MS, respectively. The total iron is reported as Fe_2O_3. PM25-A1 and PM25-A3 are representative host basalt samples. Mg-number = Mg/(Mg + Fe).

Sample:	PM25-5	PM25-9	PM25-12	PM25-15	PM25-17	PM25-18	PM25-21	PM25-22	PM25-25	PM25-26	PM25-27	PM25-28	PM25-30	PM25-31	PM25-34	PM25-35	PM25-38	PM25-A1	PM25-A3
SiO_2	44.23	43.81	43.65	43.79	44.11	43.36	–	44.26	43.84	44.01	43.52	44.48	44.17	43.54	43.86	43.49	43.43	47.39	47.32
TiO_2	0.14	0.10	0.11	0.11	0.12	0.10	–	0.13	0.12	0.13	0.11	0.14	0.12	0.11	0.12	0.10	0.10	2.80	2.85
Al_2O_3	3.70	3.05	3.26	3.13	3.51	2.91	–	3.24	3.42	3.28	2.94	3.86	3.53	2.93	3.22	3.01	2.69	13.79	14.13
Fe_2O_3	9.68	9.92	8.93	8.65	9.56	9.87	–	9.73	9.52	9.78	9.07	8.94	9.09	9.37	9.23	9.22	9.83	12.15	12.09
MnO	0.14	0.14	0.13	0.12	0.13	0.14	–	0.13	0.13	0.14	0.13	0.13	0.13	0.14	0.13	0.13	0.13	0.17	0.17
MgO	38.26	39.63	39.15	39.79	38.46	40.32	–	38.79	38.90	38.57	39.48	38.01	38.41	39.93	38.57	40.35	40.41	10.29	9.74
CaO	3.07	2.73	2.65	2.68	3.05	2.46	–	2.83	2.70	2.85	2.60	3.29	3.06	2.65	2.74	2.62	2.43	8.91	8.79
Na_2O	0.26	0.19	0.22	0.21	0.26	0.20	–	0.22	0.25	0.24	0.21	0.26	0.26	0.19	0.22	0.18	0.17	3.07	3.23
K_2O	0.02	0.02	0.02	0.02	0.01	0.03	–	0.02	0.03	0.03	0.02	0.01	0.02	0.02	0.02	0.02	0.03	1.08	1.09
P_2O_5	0.02	0.02	0.02	0.02	0.02	0.02	–	0.02	0.02	0.02	0.01	0.02	0.02	0.02	0.01	0.01	0.02	0.54	0.55
Total	99.50	99.62	98.14	98.52	99.23	99.41	–	99.37	98.93	99.04	98.10	99.14	98.80	98.91	98.11	99.13	99.24	100.20	99.96
Mg-number	88.67	88.78	89.66	90.10	88.85	89.00	–	88.76	89.00	88.64	89.60	89.38	89.32	89.40	89.22	89.65	89.05	62.64	61.46
LOI%	0.69	0.91	0.75	8.76	0.41	0.57	–	0.52	1.18	0.37	0.47	0.60	0.74	0.46	0.59	0.47	0.79	–	–
V	89	64	66	74	75	62	78	69	69	71	62	82	83	68	65	65	65	234	236
Cr	3088	2830	2994	3002	2909	2538	2982	2908	2957	2773	3046	2990	3052	3013	2802	2779	2547	308	311
Ni	1893	2184	2033	2041	2050	2186	2199	2083	2037	2029	2168	1992	1994	2082	2083	2066	2222	228	208
Co	176	104	118	114	119	162	126	186	123	142	127	111	173	130	135	94	102	49	48
Cu	24	21	19	28	28	21	21	21	27	24	20	32	28	19	25	21	24	–	–
Zn	22	32	32	27	35	26	25	28	24	31	27	21	29	29	20	28	26	127	122
Rb	3.29	2.23	1.25	3.09	5.76	8.75	4.40	3.24	4.11	3.46	6.73	3.74	0.83	6.48	2.28	0.85	3.41	16.89	16.46
Sr	31.94	21.33	15.57	20.81	16.68	18.79	27.48	23.36	17.90	27.97	18.69	17.25	17.46	17.57	20.12	21.41	15.56	654.87	644.07
Y	7.03	4.14	5.16	4.25	3.75	4.59	5.76	3.82	5.52	4.86	3.94	4.61	3.55	3.44	4.74	4.71	3.59	26.38	25.00
Zr	18.77	9.80	8.99	11.09	8.75	10.49	11.56	9.97	9.24	11.38	11.39	10.25	9.91	10.63	16.09	9.93	11.01	205.45	198.74
Nb	0.26	0.12	0.13	0.20	0.07	0.22	0.15	0.11	0.09	0.43	0.19	0.24	0.19	0.17	0.11	0.14	0.16	41.72	44.12
Sn	0.62	0.21	0.16	0.27	0.90	0.20	0.66	0.18	0.19	0.32	0.23	0.13	0.39	0.40	0.21	0.42	0.15	–	–
Cs	0.07	0.14	0.02	0.12	0.05	0.06	0.06	0.12	0.07	0.08	0.02	0.06	0.11	0.01	0.05	0.05	0.02	0.26	0.30
Ba	2.79	20.12	9.23	2.47	10.53	23.77	23.01	16.66	17.94	12.49	3.49	8.05	15.55	3.36	9.24	1.78	13.54	246.61	242.22
La	0.65	0.71	0.99	0.46	0.67	1.73	1.21	0.73	1.63	1.50	0.71	1.11	1.02	0.60	1.20	0.45	0.77	28.60	28.62
Ce	1.92	1.86	2.51	1.20	1.59	4.22	2.81	1.80	3.57	3.51	1.75	2.83	2.23	1.50	3.11	1.22	1.95	56.57	56.49
Pr	0.34	0.29	0.40	0.21	0.25	0.57	0.44	0.25	0.49	0.47	0.25	0.43	0.33	0.22	0.49	0.22	0.31	7.29	7.29
Nd	1.90	1.28	1.71	1.10	1.15	2.32	2.02	1.18	2.34	1.95	0.14	0.16	0.12	0.13	0.17	0.10	0.13	2.43	2.46
Sm	0.62	0.43	0.58	0.42	0.36	0.64	0.66	0.41	0.63	0.56	1.18	1.77	1.28	1.12	2.08	1.08	1.21	32.62	32.91
Eu	0.21	0.14	0.19	0.16	0.15	0.22	0.23	0.16	0.18	0.19	0.34	0.46	0.38	0.34	0.54	0.33	0.37	7.72	7.44
Gd	1.02	0.54	0.68	0.60	0.49	0.73	0.86	0.58	0.80	0.71	0.56	0.66	0.49	0.45	0.71	0.52	0.54	6.42	6.53
Tb	0.20	0.11	0.12	0.11	0.10	0.13	0.17	0.12	0.14	0.13	0.11	0.12	0.09	0.09	0.12	0.10	0.10	1.03	0.97
Dy	1.25	0.79	0.88	0.75	0.70	0.88	1.09	0.70	0.95	0.89	0.73	0.87	0.65	0.62	0.82	0.68	0.66	5.42	5.09
Ho	0.30	0.17	0.21	0.17	0.14	0.20	0.25	0.15	0.21	0.18	0.16	0.19	0.13	0.14	0.18	0.17	0.16	0.99	0.99
Er	0.92	0.56	0.65	0.51	0.45	0.58	0.78	0.50	0.61	0.54	0.45	0.58	0.45	0.42	0.57	0.50	0.52	2.31	2.19
Tm	0.13	0.08	0.11	0.08	0.07	0.09	0.12	0.08	0.09	0.09	0.08	0.09	0.07	0.07	0.09	0.08	0.08	0.29	0.28
Yb	0.87	0.55	0.70	0.53	0.48	0.65	0.78	0.51	0.59	0.63	0.51	0.60	0.49	0.45	0.57	0.53	0.50	1.80	1.80
Lu	0.14	0.09	0.11	0.08	0.07	0.10	0.12	0.08	0.09	0.09	0.08	0.09	0.08	0.07	0.09	0.08	0.08	0.23	0.23
Hf	1.03	0.52	0.55	0.60	0.73	0.50	0.55	1.17	0.51	0.45	1.39	0.61	0.34	1.17	0.39	0.44	1.36	4.49	4.40
Ta	0.03	0.02	0.02	0.02	0.01	0.02	0.02	0.02	0.01	0.03	0.02	0.03	0.02	0.01	0.01	0.01	0.01	2.01	2.06
W	1.48	0.40	1.12	0.71	0.98	3.57	0.16	1.49	0.54	0.35	–	0.06	1.29	0.92	0.53	0.17	2.38	–	–
Pb	0.27	0.23	0.25	0.20	0.15	0.28	0.19	0.19	0.21	0.21	0.15	0.17	0.15	0.13	0.20	0.18	0.14	1.55	1.56
Th	0.10	0.12	0.24	0.08	0.10	0.51	0.58	0.11	0.24	0.22	0.19	0.11	0.11	0.14	0.38	0.45	0.37	3.02	2.98
U	0.06	0.08	0.07	0.08	0.04	0.13	0.20	0.05	0.07	0.13	0.06	0.09	0.10	0.09	0.10	0.13	0.10	0.74	0.72

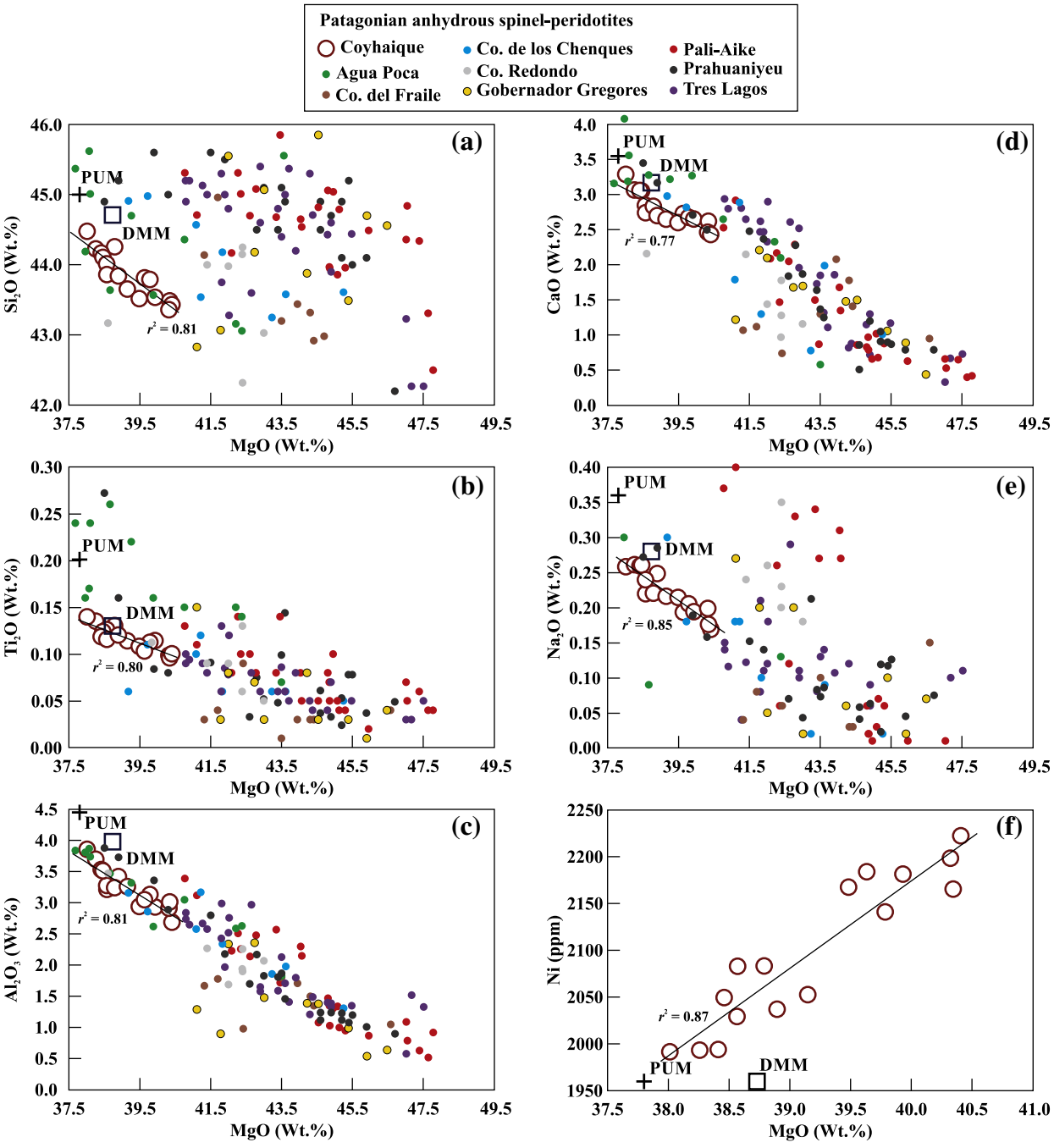

Fig. 5. Whole-rock MgO variation diagrams with correlation coefficients (r^2 = 0.77–0.87) for selected major elements (wt.%) and Ni (ppm) of the Coyhaique lherzolites (a–f). The negative correlations between MgO and the main oxides vary from fertile (close to PM) to slight refractory compositions and indicate variable degrees of partial melting. Ni is positively correlated with MgO, consistent with its compatible character during melt-peridotite equilibrium (f). For comparison, values of the primitive mantle (PM; McDonough and Sun, 1995) and depleted MORB mantle (DMM; Workman and Hart, 2005) are shown. Also plotted are Patagonian whole-rock spinel-peridotites from: Agua Poca (Jalowitzki et al., 2010), Cerro del Fraile (Kilian and Stern, 2002; Rivalenti et al., 2004; Schilling et al., 2017), Cerro de los Chenques (Rieck et al., 2007; Rivalenti et al., 2004), Cerro Redondo (Schilling et al., 2005), Gobernador Gregores (Gorring and Kay, 2000; Jalowitzki et al., 2016; Mundl et al., 2015; Rivalenti et al., 2004; Schilling et al., 2017), Pali-Aike volcanic field (Gervasoni et al., 2012; Jalowitzki et al., 2016; Mundl et al., 2015), Prahuaniyeu (Bjerg et al., 2009), and Tres Lagos (Mundl et al., 2015; Ntaflos et al., 2007; Rivalenti et al., 2004; Schilling et al., 2017).

spinel-peridotites from Patagonia are limited to only a few samples. Fig. 8c–f demonstrates that some samples from Cerro Redondo (Schilling et al., 2005) have compositional ranges for $^{206}Pb/^{204}Pb$ and $^{208}Pb/^{204}Pb$ that are similar to Coyhaique spinel-lherzolites, but with higher $^{207}Pb/^{204}Pb$ ratios. Finally, the Sr–Nd–Pb isotope data reveal that the host basalt has lower $^{87}Sr/^{86}Sr$ at a given $^{143}Nd/^{144}Nd$, as well as considerably higher $^{(206-207-208)}Pb/^{204}Pb$ ratios than the Coyhaique peridotites (Fig. 8).

4.2. Host basalt

Whole-rock major and trace element data (including REEs), Sr–Nd–Pb isotopic compositions, and K–Ar ages for two representative samples of the lava hosting mantle xenoliths are presented in Tables 1, 2 and 3, respectively. The Coyhaique host lava is classified as a basalt with idiomorphic olivine and clinopyroxene phenocrysts. The fine-grained groundmass consists of olivine, clinopyroxene, plagioclase, oxides,

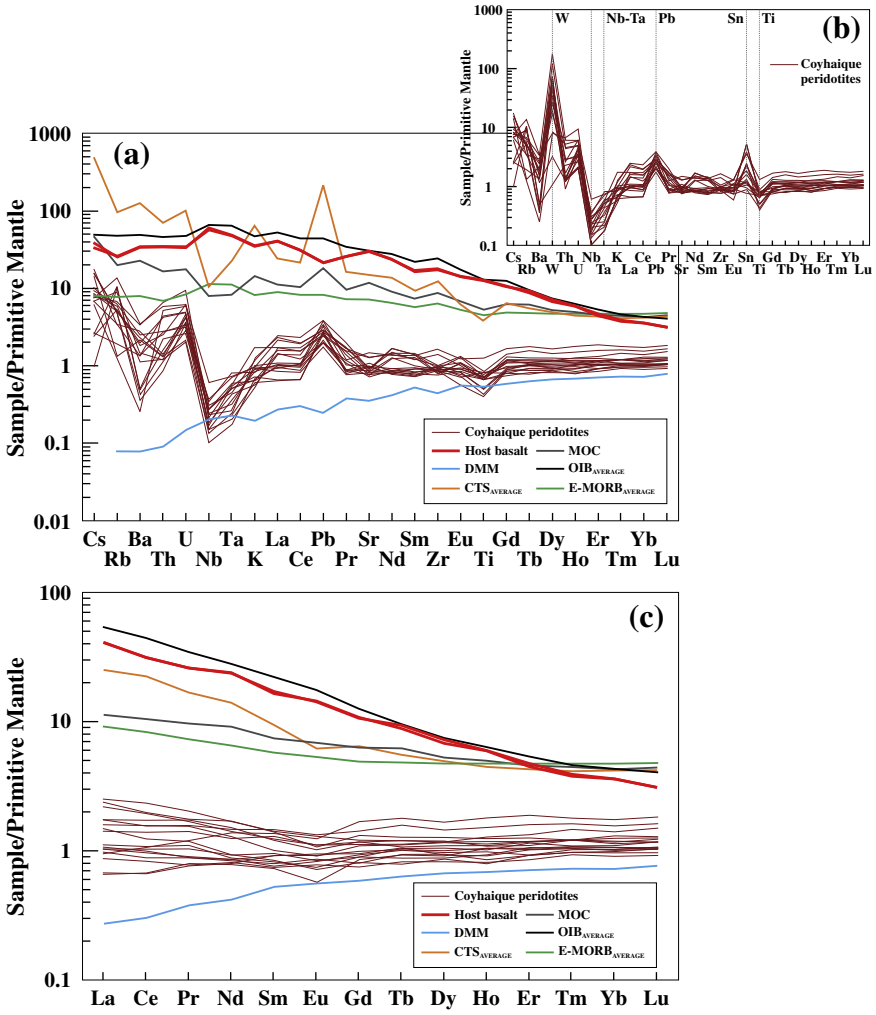

Fig. 6. Primitive mantle-normalized incompatible trace elements (a, b) and REE (c) diagrams of the whole-rock mantle xenoliths using the normalization values of Sun and McDonough (1989). For comparison, values of the host basalt, depleted MORB mantle (DMM; Workman and Hart, 2005), modified oceanic crust (MOC is represented by Chile Ridge metabasalt, sample D42-4, Segment 3; Karsten et al., 1996), Chile Trench sediments average (CTS; Jacques et al., 2013; Kilian and Behrmann, 2003; Lucassen et al., 2010; Shinjoe et al., 2013), as well as OIB and E-MORB averages (Sun and McDonough, 1989) are shown.

glass, and rare alkali feldspar. The lava is relatively fresh, with incipient alteration of some olivine phenocrysts along their rims, which were partially replaced by iddingsite.

The lava is classified as alkaline basalt, based on its SiO_2 (~47.3 wt.%) and alkali ($Na_2O + K_2O$ ~4 wt.%) contents. The basalt has high Mg-number [Mg# = atomic Mg/(Mg + Fe) × 100] (>61) and MgO values (~10 wt.%), as well as high Cr and Ni contents (averages of 309 and 218 ppm, respectively). The host basalt also contains high TiO_2 (>2.8 wt.%) contents associated with high Ce/Yb_N (8.7), Nb/Ta (>20), Ce/Pb (>36), Nb/U (>56), and Nb/Nb* (>1.5) ratios and low La/Nb (<0.7) ratios, similar to intraplate basalts from continental and oceanic settings worldwide. Th/Yb vs. Nb/Yb (Pearce, 2008) and Nb/Y vs. Zr/Y (Fitton et al., 1997) trace element ratio diagrams, as well as delta Nb [$\Delta Nb = 1.74 + \log(Nb/Y) - 1.92 \log(Zr/Y)$; Fitton et al., 1997] values, also indicate that our samples are OIB-like basalts because they plot in the field of OIBs in both diagrams (not shown) and have $\Delta Nb > 0$ ($\Delta Nb = 0.23$ and 0.26). In addition, the Coyhaique host basalt is characterized by slight depletion in highly incompatible and fluid-mobile trace elements (Rb, K, and Pb; Fig. 6a), and by elemental ratios similar to average HIMU-OIB values (e.g., K/Nb = 205–213, Zr/Nb = 4.5–4.9, Th/Nb = 0.07, and Ba/Nb = 5.5–5.9; Weaver, 1991).

The non-modal batch melting equation of Shaw (2006) [$C_i^L = C_i^S/(D_i + F(1 - P_i))$] was applied to estimate the degree of partial melting that generated the lava from Coyhaique. For calculations, we used the following definitions: C_i^L is the concentration of trace element i in liquid, C_i^S is the concentration of trace element i in solid, D_i is the distribution coefficient of i between solid and liquid, F is the fraction of liquid (melt), and P_i is the distribution coefficient of i for assemblage entering the liquid. The fractionated HREE ratios (e.g., $Tb/Yb_N = 2.45–2.60$) suggest that this basalt was generated by a small degree of partial melting (up to 6%, not shown) within the garnet stability field.

Isotopically, the host basalt has relatively low initial ($_i$) $^{87}Sr/^{86}Sr$ (0.703039–0.703058), coupled with high $^{143}Nd/^{144}Nd_i$ (0.512874–0.512880), and $^{206}Pb/^{204}Pb$ (19.333–19.389), $^{207}Pb/^{204}Pb$ (15.677–15.679), $^{208}Pb/^{204}Pb$ (39.353–39.358) isotope ratios. The age correction applied to the Sr-Nd isotopic ratios was determined based on their respective whole-rock K–Ar dates, determined in this study, which yielded 53.6 ± 2.9 Ma and 53.7 ± 2.9 Ma (uncertainties are 1σ, Table 3). These ages are broadly consistent with those reported by Morata et al. (2000) (58.6 ± 2.0 Ma).

The Sr–Nd isotopic signatures of the host basalt require a depleted component because it plots between depleted MORB mantle (DMM; Workman and Hart, 2005) and HIMU-OIBs (e.g., Hanyu et al., 2014) (Fig. 8a). The Sr isotope ratios for these samples are slightly lower at a given Nd isotopic composition compared to the HIMU-like Pali-Aike Volcanic Field basalts ($^{87}Sr/^{86}Sr = 0.703160–0.703511$, $^{143}Nd/^{144}Nd = 0.512883–0.512944$, and $^{206}Pb/^{204}Pb = 18.790–19.170$; Choo et al., 2012; D'Orazio et al., 2000; Stern et al., 1990) but fall within the

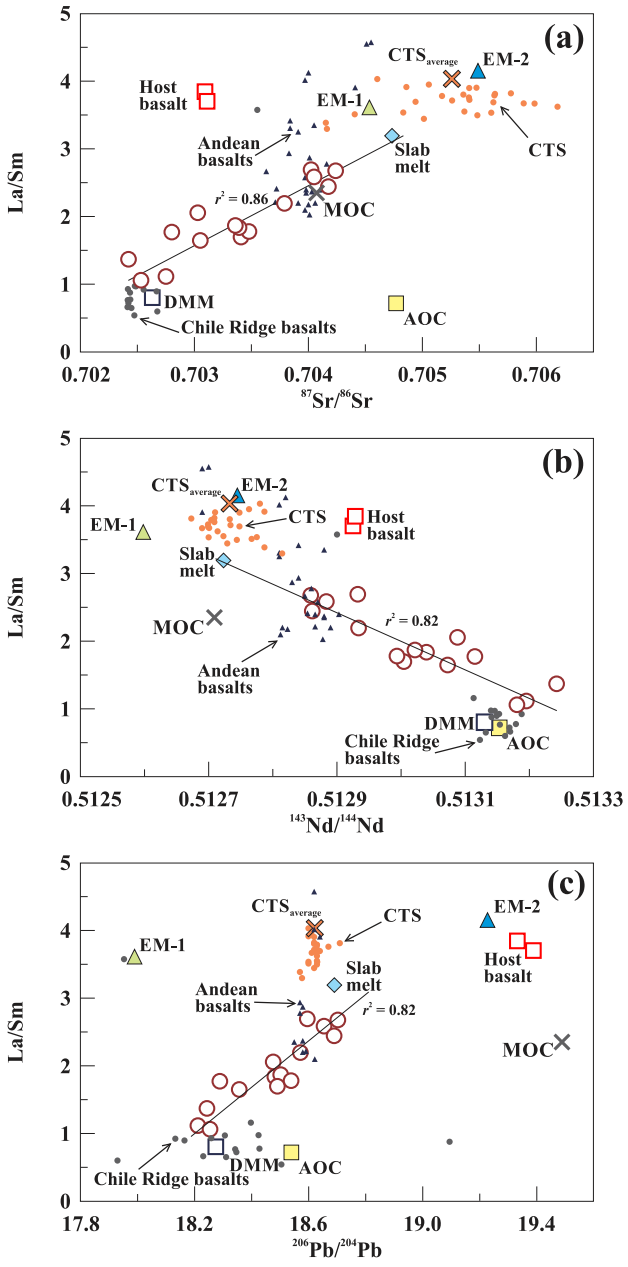

Fig. 7. La/Sm ratio vs. Sr–Nd–Pb isotopic ratios for Coyhaique peridotites, showing a good correlation (r^2 = 0.82–0.86) between the depleted mantle and a slab-derived melt (see text for details). Shown for comparison are the host basalt, depleted MORB mantle (DMM), modified oceanic crust (MOC), Chile Trench sediments (CTS), altered oceanic crust (AOC), enriched mantle reservoirs (EM-1 and EM-2), Andean volcanic arc basalts, Chile Ridge basalts, and slab melt (50% CTS + 50% MOC) (see text for references).

range of HIMU-like Antarctic Peninsula basalts ($^{87}Sr/^{86}Sr$ = 0.702690–0.703360, $^{143}Nd/^{144}Nd$ = 0.512823–0.512994, and $^{206}Pb/^{204}Pb$ = 18.793–19.282; Hole, 1990; Hole et al., 1993). In terms of Pb isotopes (Fig. 8e, f), the host basalt has higher $^{(206-207-208)}Pb/^{204}Pb$ ratios than those of both Pali-Aike and Antarctic basalts (Choo et al., 2012; Hole et al., 1993; Stern et al., 1990), almost reaching the Chile Ridge modified oceanic crust composition (MOC; Karsten et al., 1996; see Section 5.3.1 for details). Although the host basalt shows more radiogenic $^{206}Pb/^{204}Pb$ compared with other HIMU-like basalts from southernmost Patagonia and Antarctic Peninsula, these ratios are significantly lower than the HIMU end-member (e.g., Sta. Helena and the Cook–Austral Islands; Hanyu et al., 2014).

The Coyhaique host basalt can be temporally and chemically correlated with the volcanic products of the Lower Basaltic Sequence (LBS) of Meseta de Chile Chico (60–34 Ma; Baker et al., 1981; Charrier et al., 1979; Espinoza et al., 2005) and with the Balmaceda plateau basalts (51–44 Ma; Baker et al., 1981; Demant et al., 1996; Parada et al., 2001). They also show affinities with the Posadas plateau basalts, which are located in the Argentinian back-arc (57–45 Ma, Kay et al., 2002; Ramos and Kay, 1992).

5. Discussion

5.1. Weathering effects on Coyhaique peridotites

The loss on ignition (LOI) data of studied samples is presented in Table 1. Most of the LOI values of Coyhaique peridotites are relatively low, ranging from 0.4 wt.% to 1.2 wt.% (average 0.6 wt.%), which indicates that secondary alteration was limited and/or the fluid content is low. However, sample PM25-15 has high LOI value (close to 9 wt.%), which can be explained by the abundant occurrence of iddingsite veins recognized in the thin section. Because there is no correlation between La/Sm and LOI values for Coyhaique peridotites (Fig. 9), and because LOI is a good parameter to discriminate between fresh and weathered samples (Chauvel et al., 2005), the lack of correlation implies that weathering did not have a significant effect on the ratios of REEs in the studied samples. Furthermore, the highest LOI value is associated with one of the lowest La/Sm ratios, consistent with this conclusion.

5.2. Partial melting and metasomatism of Coyhaique peridotites

Compared to PM and DMM compositions, most of the spinel-lherzolites studied here show depletion in SiO_2, TiO_2, Al_2O_3, CaO, and Na_2O coupled with relative enrichment in MgO, which can be explained by variable degrees of partial melting of a fertile primitive mantle (e.g., McDonough and Sun, 1995) (Fig. 5a–e). Despite this, the high and variable HREE contents of the Coyhaique lherzolites (e.g., Yb_N = 0.92–1.77; most >1.0) are difficult to explain by progressive melt depletion of a spinel-peridotite source, which results in depleted REE relative to primitive mantle. Garnet is by far the most important HREE host in mantle xenoliths (e.g., Ionov et al., 2005 and references therein). However, our samples are garnet-free, and there is no petrographic evidence (e.g., symplectite texture) suggesting that the SCLM beneath Coyhaique was previously stable at a deeper-level, in the garnet stability field. In contrast, the HREE are mainly controlled by clinopyroxene in spinel-peridotites. Thus, although HREE patterns are unexpected given the variable degrees of melt depletion observed in most samples, they are compatible with the high modal contents of clinopyroxene (>10%; Table A.2).

The extent of partial melting (F) can be evaluated using the non-modal batch melting equation reported by Shaw (2006) [$C^S = ((D-PF)C)/((1-F)(D+F(1-P))$] (see definitions of parameters in this equation in Section 4.2). The REEs were selected to calculate F because they have a similar behaviour during partial melting due to their similar bulk partition coefficients. Moreover, the REEs are less disturbed by cryptic metasomatism in comparison with the other incompatible elements. We modelled partial melting using both PM (Sun and McDonough, 1989) and DMM (Workman and Hart, 2005) as starting compositions in the spinel stability field (Fig. 10a, b). The modal and chemical compositions employed here for PM and DMM are from McDonough (1990) and Workman and Hart (2005), respectively. The mineral/melt partition coefficients for the REEs are taken from Niu and Hékinian (1997) and Shaw (2006), whereas the mineral melting modes are those of Johnson (1998).

The geochemical modelling using the REE abundances fails to reproduce the REE patterns of the Coyhaique spinel-lherzolites based on simple partial melting of spinel-facies, fertile mantle peridotite (PM-like) or depleted mantle peridotite (DMM) (Fig. 10a, b). This indicates a complex history of incompatible element depletion and/or enrichment related to partial melting and metasomatic events. For the

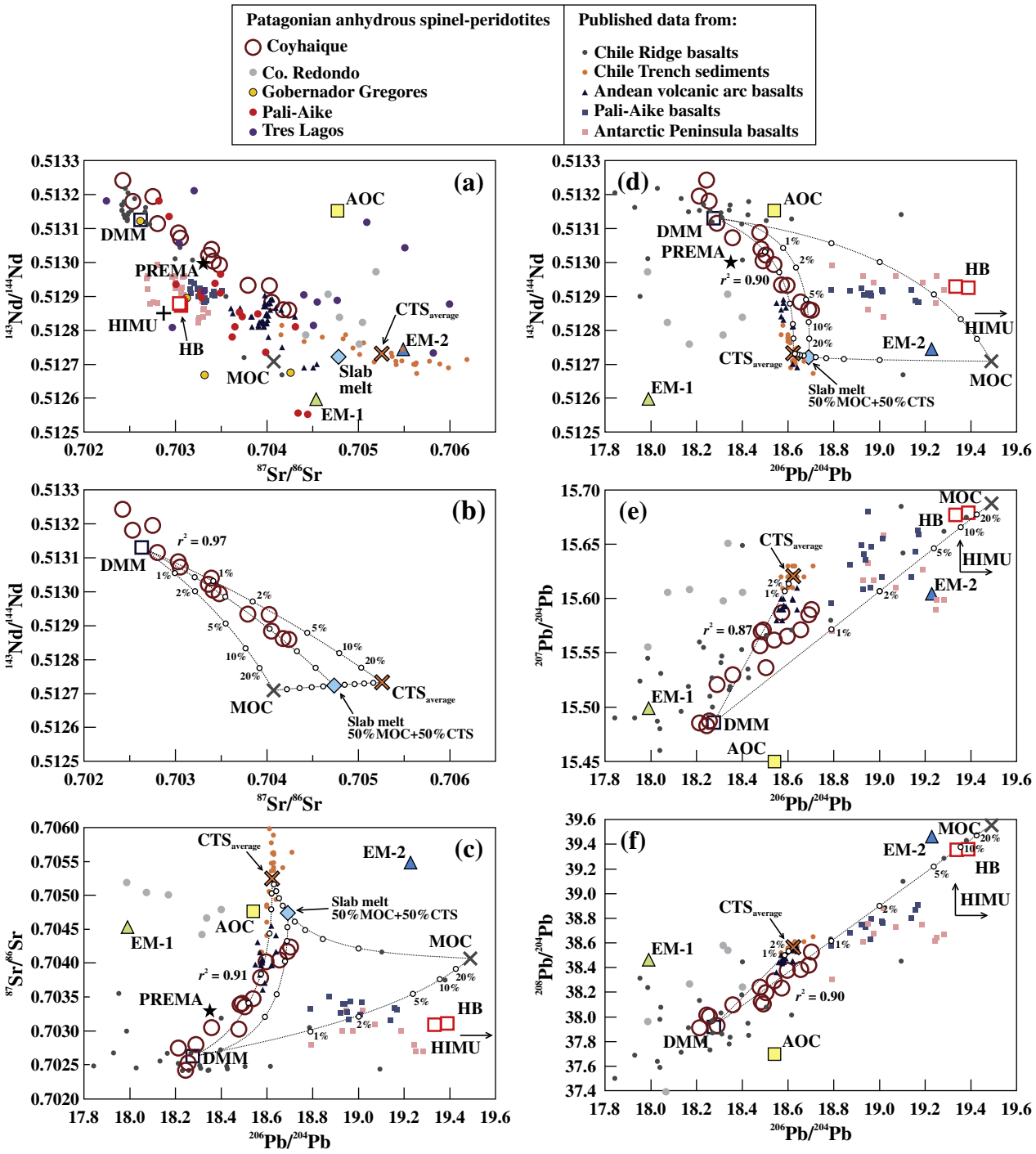

Fig. 8. $^{87}Sr/^{86}Sr$ vs. $^{143}Nd/^{144}Nd$ (a, b) and Sr–Nd–Pb vs. $^{206}Pb/^{204}Pb$ (c–f) isotope variations of whole-rock selected Coyhaique spinel-lherzolites. The data for comparison are indicated in the text. The dashed line represents mixing between the depleted MORB mantle (DMM; Workman and Hart, 2005) and slab melt (50% CTS + 50% MOC). Mixing lines for Coyhaique peridotites together with these two end-members show good correlations (r^2 = 0.90–0.97). The mixing lines between the DMM and slab melt are marked at intervals of 1%, 2%, 5%, 10%, and 20% (white filled circles), with increasing contributions from the latter component. Mixing lines between the two slab-derived components (CTS and MOC) are marked at intervals of 10%, 20%, 30%, 40%, 50%, 60%, 70%, 80%, and 90%.

modelling, we chose a mixture of 90% PM (Sun and McDonough, 1989) and 10% slab-derived component (50% Chile Trench sediments + 50% modified oceanic crust) as a source because HREE patterns of our samples that are relatively flat, similar to those of the primitive mantle (Fig. 6c). Using this source, the model estimates that the spinel-lherzolites are residues formed after <8% of non-modal batch melting (Fig. 10c). It is important to note that three samples with HREE higher than the estimated source composition are clinopyroxene-rich lherzolites (Cpx >18.5%; Table A.2), which probably record modal metasomatism.

5.3. Involvement of slab-derived components in the SCLM

The spinel-lherzolites studied here have a chemical signature that is typical of most arc magmas in terms of the trace element compositions, such as high ratios of LILE/(HFSE-REE) and strong negative Nb, Ta, and

Table 2
Whole-rock Rb–Sr, Sm–Nd and Pb–Pb isotopic data for Coyhaique mantle xenoliths analysed in this study plus two samples of the host basalt (PM25-A1 and PM25-A3). The numbers in the parentheses indicate the 2σ uncertainties in the last digits.

Sample	Rb	Sr	$^{87}Sr/^{86}Sr$	Sm	Nd	$^{143}Nd/^{144}Nd$	εNd	$^{206}Pb/^{204}Pb$	$^{207}Pb/^{204}Pb$	$^{208}Pb/^{204}Pb$
PM25-5	0.38	15.63	0.702531(13)	3.69	17.64	0.513181(14)	+10.6	18.255(08)	15.487(07)	38.007(16)
PM25-9	0.91	12.74	0.703052(11)	2.63	17.06	0.513073(17)	+8.5	18.358(16)	15.530(14)	38.100(34)
PM25-12	0.18	10.25	0.703410(07)	2.51	10.66	0.513005(16)	+7.1	18.491(4)	15.571(04)	38.107(09)
PM25-15	0.29	14.37	0.702750(06)	2.96	13.54	0.513195(06)	+10.9	18.212(4)	15.486(04)	37.914(09)
PM25-17	0.17	11.14	0.703359(13)	3.29	17.08	0.513022(15)	+7.5	18.503(15)	15.537(12)	38.199(31)
PM25-21	0.36	11.27	0.703392(12)	3.14	14.22	0.513040(12)	+7.8	18.482(04)	15.570(04)	38.125(08)
PM25-22	0.83	12.88	0.702802(12)	8.37	15.52	0.513155(11)	+9.3	18.289(15)	15.521(13)	37.932(30)
PM25-25	0.13	6.81	0.704050(14)	7.49	15.03	0.512883(07)	+4.8	18.655(19)	15.572(16)	38.386(39)
PM25-26	0.29	14.37	0.704024(09)	3.33	30.46	0.512932(13)	+5.7	18.596(03)	15.566(02)	38.380(05)
PM25-27	0.33	9.82	0.703030(04)	3.23	15.82	0.513088(14)	+8.8	18.477(06)	15.557(05)	38.243(12)
PM25-28	0.49	13.41	0.704175(09)	4.19	22.90	0.512862(09)	+4.4	18.690(09)	15.585(08)	38.422(19)
PM25-30	0.48	16.65	0.704239(10)	2.81	15.59	0.512859(12)	+4.3	18.703(06)	15.590(05)	38.524(12)
PM25-31	0.07	11.14	0.703479(10)	3.34	24.94	0.512994(06)	+6.9	18.539(07)	15.562(06)	38.294(15)
PM25-34	0.09	6.66	0.703791(04)	2.58	11.97	0.512934(16)	+5.8	18.572(04)	15.587(03)	38.236(08)
PM25-35	0.23	11.62	0.702422(12)	2.40	9.46	0.513242(12)	+11.8	18.244(05)	15.483(04)	38.017(11)
PM25-A1[a]	16.89	654.87	0.703112(15)	7.72	32.62	0.512925(06)	–	19.333(04)	15.677((03)	39.353(16)
PM25-A1[b]	–	–	0.703058(15)	–	–	0.512874(06)	+5.6	–	–	–
PM25-A3[a]	16.46	644.07	0.703094(09)	7.44	32.91	0.512929(07)	–	19.389(04)	15.679(02)	39.358(15)
PM25-A3[b]	–	–	0.703039(09)	–	–	0.512880(07)	+5.7	–	–	–

For host basalts, initial Sr and Nd isotope compositions were calculated using the respective K–Ar ages of each sample (see Table 3). Parent/daughter isotope ratios were recalculated using Rb, Sr, Sm and Nd concentrations from Table 1.
[a] Measured isotopic ratios.
[b] Age corrected isotopic ratios (initial ratios).

Table 3
Whole-rock analytical data for the unspiked K–Ar ages of the host basalt.

Sample	K (wt.%)	^{40}Ar rad ($10^{-8}cm^3STP/g$)	$^{38}Ar/^{36}Ar$	Age (Ma)	Air fraction (%)
PM25-A1	0.92 ± 0.02	193.84 ± 9.71	0.1893 ± 0.0010	53.7 ± 2.9	43.0
PM25-A3	0.84 ± 0.02	176.82 ± 8.86	0.1895 ± 0.0007	53.6 ± 2.9	41.7

For calculation of ^{40}Ar rad, ($^{40}Ar/^{36}Ar$) initial = 296.0 is assumed. Error: 1σ.

Ti anomalies. There are several potential agents and processes capable of modifying the lithospheric mantle composition and impart compositional characteristics commonly found on melts formed at subduction zones: 1) dehydration of subducted oceanic crust (including altered oceanic crust) and sediments, 2) accretion of sediments derived from the continental crust and oceanic seafloor, 3) slab melts (e.g., adakites) produced from the partial melting of subducted oceanic crust, 4) lower crust delamination, and 5) asthenospheric upwelling through slab windows.

Typical fluid-mobile (e.g., LILE) over fluid-immobile (e.g., HFSE and REE) trace element ratios are useful to estimate the proportion of slab-derived components into the mantle. To evaluate the characteristics of the metasomatic component that affected the Coyhaique peridotites, we employed the (Pb–Th)/Ce, (Ba–U–Pb–Sr)/Th, Th/Yb, Sr/Y and La/(Sm–Yb) ratios, as well as Sr–Nd–Pb isotopes (Figs. 7, 8, and 11, not all of the ratios are shown). We consider several scenarios to identify the potential metasomatic component of the SCLM beneath the Coyhaique locality. These scenarios involve aqueous fluids and/or melts derived from dehydration, and/or melting of the down-going southeast Pacific oceanic crust and Chile Trench sediments, which may be associated with the subduction of Farallón–Aluk spreading ridge during the Paleocene to Eocene or with an even older subduction-related event.

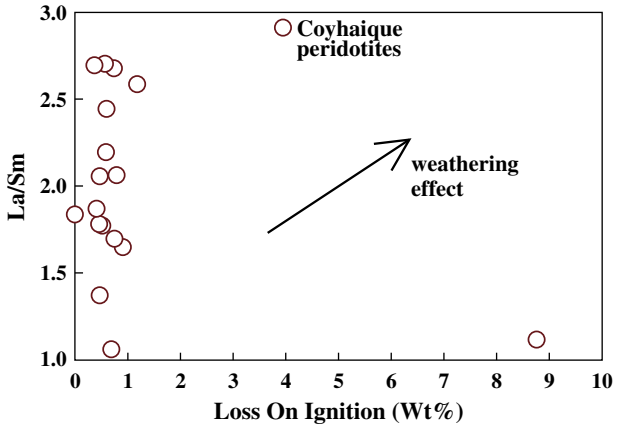

Fig. 9. La/Sm vs. loss on ignition for Coyhaique peridotites showing that there is no positive correlation between them, which suggests that weathering did not have a significant effect on the ratios of REEs in the studied samples.

5.3.1. Sediments and oceanic crust

The oceanic crust (altered or not) and overlying sediments contribute important input fluxes to the subduction system. Because subducted sediments have much higher ratios of certain trace element pairs [e.g., (Th–Ce)/Yb, Th/Sr, La/Sm, and Pb/Ce], and higher Sr–Pb and lower Nd isotopic ratios than those of altered oceanic crust, it is possible to model the contribution of oceanic crust, including altered oceanic crust (Hauff et al., 2003; Staudigel et al., 1996), and the overlying layer of subducted sediments into the SCLM beneath the Coyhaique locality.

Our results suggest that the Coyhaique spinel-lherzolites were variably modified by slab melts released from a combination of sediments and oceanic crust, precluding the involvement of significant amounts of altered oceanic crust (Figs. 7, 8, and 11). Thus, compositions of Chile Trench sediments (CTS; Jacques et al., 2013; Kilian and Behrmann, 2003; Lucassen et al., 2010; Shinjoe et al., 2013) and Chile Ridge oceanic crust (metabasaltic sample D42-4, Segment 3; Karsten et al., 1996) were employed in the following quantitative models.

In Fig. 8, a sample of Chile Ridge metabasalt is labelled as a modified ocean crust (MOC) (Karsten et al., 1996). This sample is thought to have been generated from the melting of a depleted mantle source with contamination of ~11.6% altered oceanic crust and ~0.4% sediments at

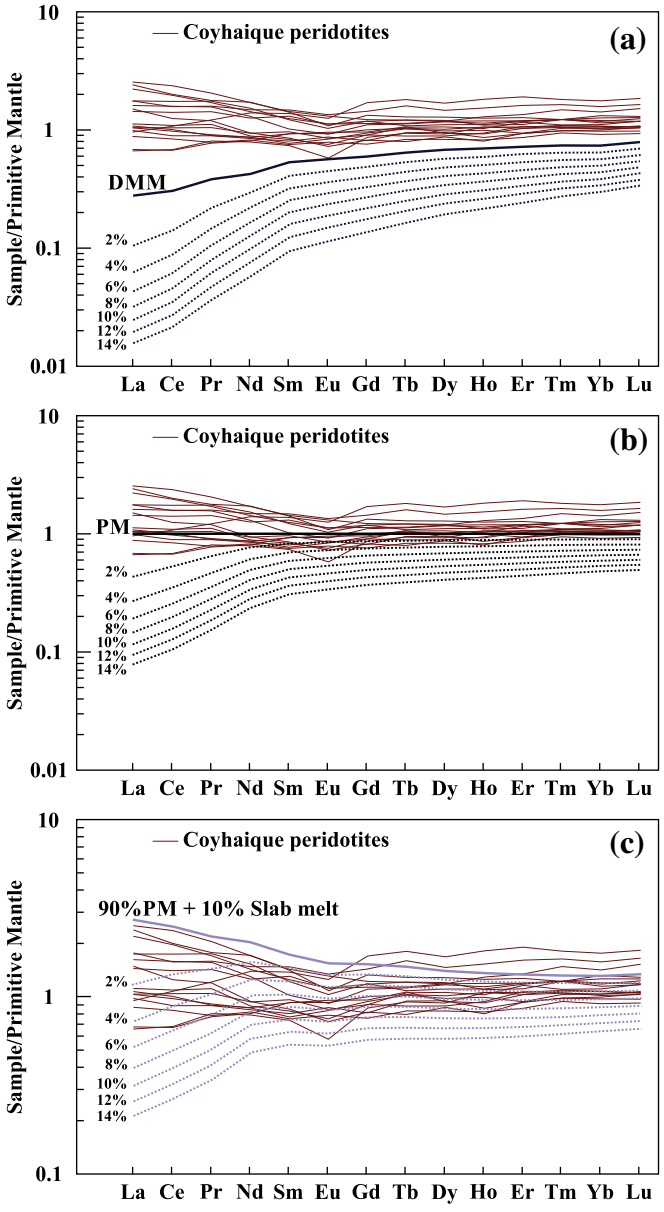

Fig. 10. Primitive mantle-normalized REE plots for Coyhaique peridotite samples and partial melt residues (dashed lines) from the spinel-facies depleted mantle (DMM; plot a), primitive mantle (PM; plot b), and metasomatized lithospheric peridotite mantle source (90% PM + 10% slab melt; plot c) compositions. Each dashed line indicates the percentage of partial melting as follows: 2%, 4%, 6%, 8%, 10%, 12%, and 14%. The source modes assumed here for partial melting are from the DMM ($Ol_{0.57}$ + $Opx_{0.28}$ + $Cpx_{0.13}$ + $Sp_{0.02}$; Workman and Hart, 2005) and PM ($Ol_{0.56}$ + $Opx_{0.22}$ + $Cpx_{0.19}$ + $Sp_{0.03}$; McDonough, 1990). The PM source mode was used for metasomatized lithospheric peridotite. The melt modes are those proposed by Johnson (1998) for spinel stability field ($Ol_{-0.06}$ + $Opx_{0.28}$ + $Cpx_{0.67}$ + $Sp_{0.11}$). Mineral/melt partition coefficients are from the compilation of Niu and Hékinian (1997) and Shaw (2006).

depth. The trace element and Sr–Nd–Pb isotopic compositions of the Chile Trench sediments are similar to those of primitive Andean volcanic arc basalts (e.g., Hickey et al., 1986; Hickey-Vargas et al., 1989), which imply significant input of terrigenous sediments eroded from materials of the Andean volcanic arc. In terms of radiogenic isotopes, the composition of the Chile Trench sediments lies largely between EM-1 and EM-2 mantle components (Fig. 8).

As shown in Fig. 8, the Coyhaique SCLM is heterogeneous in Sr–Nd–Pb isotopic compositions, containing both depleted (DMM) and enriched (slab melt) components. Thus, mixing lines between two end-members may be used to account the contribution of different slab-derived components. Figs. 8 and 11 show trace elements and isotope ratios for the resulting mixtures. They support all data for the Coyhaique spinel-lherzolites when up to 10% of slab component is added to the depleted mantle (>90% DMM). On the Sr vs. Nd and Sr–Nd vs. Pb isotope diagrams (Fig. 8), the studied samples define an excellent correlations (r^2 = 0.90–0.97) between DMM and a mixing of modified oceanic crust (MOC) and Chile Trench sediments in a proportion of 50:50. Mixing arrays observed in the Pb/Ce vs. Pb and Th/Yb vs. Sr/Th diagrams indicate that less than 10% of slab melt is necessary to explain most of studied samples (Fig. 11), but the relationship between these ratios is most easily explained by mantle heterogeneity related to variable contributions from DMM, sediments and oceanic crust. Considering that some Coyhaique peridotites have even lower Sr/Th ratios compared to the average of Chile Trench sediments, we used a pelagic sediment from the Antarctic plate (sample 78; Kilian and Behrmann, 2003) to calculate a mixing line for our samples (Fig. 11b). On Pb isotope diagrams (Fig. 8e, f), the spinel-lherzolites show good positive correlations (r^2 = 0.87–0.90), with the more radiogenic samples containing similar isotope ratios to those of the sediments and Andean volcanic arc basalts. This suggests that most of the Pb budget of these samples must come from the sediments. Conversely, the less radiogenic samples overlap with the DMM end-member.

Labanieh et al. (2012) showed that addition of sediments to the mantle wedge controls the La/Sm ratio of the mantle source. In order to obtain the best-fit correlation line reflecting two-component mixing between DMM and slab melt end-members, we plotted the Sr–Nd–Pb isotopes against La/Sm ratios for all studied spinel-peridotites. Well-defined linear trends (r^2 = 0.82–0.86) between the depleted mantle and the slab-derived melt were obtained and support the previous results (Fig. 7).

5.3.2. Dehydrated fluids from the subducted sediments and oceanic crust

As mentioned above, the geochemical and isotope signatures of the Coyhaique spinel-lherzolites can be attributed to their interaction with melts from subducted sediments and oceanic crust. However, we cannot rule out a metasomatic contribution from dehydration of the subducted slab. Dehydration of a slab produces an enrichment of the highly incompatible chalcophile elements (e.g., W, Pb and Sn) as well as elevated (Rb–Ba–U–Sr)/Th ratios because Rb, Ba, U and Sr are preferentially incorporated into the fluid phases, whereas Th is released efficiently from the slab only when sediment melts are involved (e.g., Hawkesworth et al., 1997). The Coyhaique spinel-lherzolites have Ba/Th (12.24–171.46; CTS = 50–400), U/Th (0.25–0.99; CTS = 0.11–0.91), Sr/Th (37.04–273.35; CTS = 19.24–138.16) and Pb/Th (0.28–2.62; CTS = 1.35–3.39) ratios that are similar to those of the Chile Trench sediments (CTS), which is consistent with cryptic metasomatism by a dehydration-induced silicate melt rather than by dehydrated fluid. The absence of modal metasomatism supports this argument because hydrated mineral phases (e.g., pargasite, phlogopite, phengite and serpentine) were not found, implying a metasomatic enrichment without a significant input of aqueous fluid. Additional support is provided by Sr isotopic ratios measured on the pore water from the Chile Trench sediments (~0.7089–0.7092; Lucassen et al., 2010). These values are considerable higher than those from whole-rock Coyhaique peridotites and Chile Trench sediments.

5.3.3. Lack of slab-derived adakitic melts

In the southern Patagonia, late Miocene to Recent adakitic magmatism and its metasomatism have been described in Cerro Pampa (Kay et al., 1993; Orihashi et al., 2013), Cook Islands (Stern and Kilian, 1996), and Cerro del Fraile (CF; Faccini et al., 2013; Kilian and Stern, 2002). In general, Sr/Y vs. Y and La/Yb vs. Yb discriminant diagrams are applied to classify adakites (e.g., Castillo, 2006). Hence, the product of adakitic metasomatism is expected to have 1) a high Sr/Y ratio with a high Sr concentration, 2) high La/Yb, 3) high SiO_2 contents with less negative Nb–Ta anomalies, and 4) low $^{87}Sr/^{86}Sr$ ratios and low MgO content

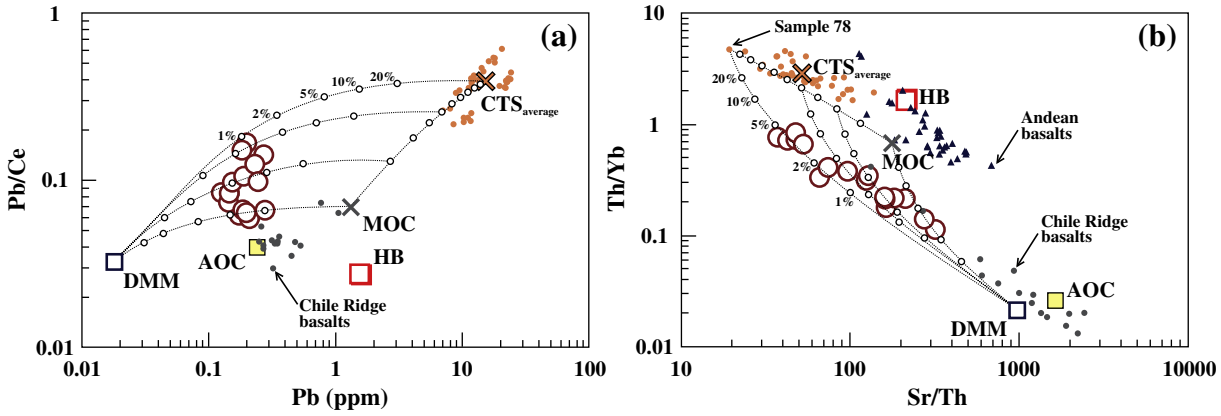

Fig. 11. Selected trace element ratio diagrams. Pb/Ce vs. Pb (a) and Th/Yb vs. Sr/Th (b) diagrams illustrate the geochemical characteristics of the Coyhaique spinel-lherzolites. For comparison, Coyhaique host basalt (HB), depleted MORB mantle (DMM), modified oceanic crust (MOC), Chile Trench sediments (CTS), Chile Ridge basalts, altered oceanic crust (AOC), and Andean volcanic arc basalts are shown. The literature data for Andean basalts employed in this work do not contain analysis of Pb. Calculated two-component mixing lines between DMM-MOC, DMM-CTS, and DMM-Slab melt are shown as dashed lines. The white filled circles along the mixing lines indicate the percentage of the metasomatic component in the mixture as follow: 1%, 2%, 5%, 10%, and 20%, with increasing contributions from the metasomatic component. Mixing lines between the two slab-derived components (CTS and MOC) are marked at intervals of 10%, 20%, 30%, 40%, 50%, 60%, 70%, 80%, and 90%. See text for references.

(e.g., Castillo, 2006; Moyen, 2009). Moreover, experimental studies have shown that adakitic melts react strongly with lherzolites, forming a new paragenesis rich in orthopyroxene, which could be found as orthopyroxene-rich veins in the SCLM (Gervasoni et al., 2017).

Mantle xenoliths from Cerro del Fraile are modified by adakite metasomatism, which produced geochemical characteristics typical of slab melts (see mixture of 94% of Xe-17 with 6% of adakitic glass from Kilian and Stern, 2002). In contrast, the Coyhaique spinel-lherzolites show a lower Sr concentration (<30 ppm; CF = 48 ppm) with a minor Sr anomaly on a multi-element diagram (Fig. 6a, b), as well as significantly lower Sr/Y (3.0–6.1; CF = 55) and La/Yb ratios (0.62–3.8; CF = 8) coupled with a slight LREE enrichment on the REE pattern (Fig. 6c). Moreover, all of the Coyhaique spinel-lherzolites have the same or more mafic compositions, e.g., lower SiO_2 and higher MgO contents, than the DMM and PM components (Fig. 5a). Based on these data, it is possible to preclude the participation of adakite melts in the process of metasomatism that is recorded in the Coyhaique mantle xenoliths.

5.4. Time constraints for the slab-derived metasomatism of the SCLM beneath Coyhaique

In tectonic settings in which slab windows beneath a back-arc region result from the subduction of spreading ridges, magmas released from the sub-slab asthenosphere are commonly assumed to be largely uncontaminated by the supra-slab mantle components and have OIB or MORB-like magma compositions (e.g., Gorring et al., 2003).

Our new K–Ar age of ~54 ± 3 Ma for the Coyhaique HIMU-like OIB host basalt is broadly consistent with the previous K–Ar age of ~59 ± 2 Ma of Morata et al. (2000). The ages suggest that this magmatism is linked to the formation of a slab window resulting from collision of the Farallón–Aluk ridge-trench against the western margin of South America at the latitude of studied area (45°46′S) during the Paleocene–Eocene (Fig. 12).

It is well known that the process of slab detachment allows the infiltration of the sub-slab asthenosphere within the slab gap and, consequently, the metasomatism of a depleted SCLM with a strong OIB or MORB-like signatures. This process probably took a few million years to occur because the enriched material needed time to be convectively transported into the SCLM. Considering that there is no petrographic or geochemical evidence that HIMU-like OIB melts from the asthenospheric slab window had much influence on the Coyhaique spinel-lherzolites, we conclude that these samples were brought to the surface during the initial stages of the Farallón–Aluk spreading ridge collision with the Chile Trench (Fig. 12). This model is supported by the low recrystallization and strain ratios, as well as by the low equilibrium temperatures (~1050 °C; Schilling et al., 2017) of studied samples: a mantle with higher temperatures would display more intensive recrystallization and strain rates than that at lower temperatures (Lloyd et al., 1997).

The Coyhaique spinel-lherzolites have Proterozoic SCLM T_{RD} model ages (1.3–1.7 Ga; Schilling et al., 2017) and subducted-related geochemical and isotopic characteristics. Thus, we suggest that the slab-derived components originated from ancient (Paleocene or older?) modified oceanic crust melt mixed with sediments subducted into the depleted SCLM. In relation to the Phanerozoic geologic evolution of Patagonia (e.g., Cawood and Buchan, 2007; Domeier and Torsvik, 2014), we cannot rule out the possibility that the SCLM beneath Coyhaique was possibly metasomatized by ancient subduction events.

5.5. Mantle source of Coyhaique lava

The Eocene alkaline basalt from Coyhaique offer a remarkable opportunity for using their trace element and isotopic compositions, as well as K–Ar ages, to evaluate their mantle source characteristics and processes of melt generation. Plate tectonic models associated with geochronological and geochemical data of Eocene OIB-like magmatism indicate subduction of the Farallón–Aluk spreading ridge beneath the south Patagonia and allowed the formation of a slab window beneath the Aysén Region during Paleocene to Eocene time (e.g., Breitsprecher and Thorkelson, 2009; Cande and Leslie, 1986; Morata et al., 2000; Parada et al., 2001; Ramos and Kay, 1992). Thus, we suggest that the host alkaline basalt was formed by small degrees of partial melting (up to 6%), probably from asthenospheric mantle upwelling through slab window related to the Farallón–Aluk ridge collision and subduction beneath south Patagonia at ~54 Ma.

The HIMU-like OIB affinity of this basalt is evident from their enrichment of Nb and Ta relative to Ba and Rb and overall depletion in Rb, Ba, Pb, and Sr relative to EM basalts. Ratios of various incompatible elements are different in EM and HIMU-type OIBs (Weaver, 1991). Incompatible element ratios of Coyhaique host basalt (K/Nb = 205–213, Rb/Nb = 0.37–0.40, Zr/Nb = 4.5–4.9, Th/Nb = 0.07, Ba/Nb = 5.5–5.9, and La/Nb = 0.65–0.69) are typical of a HIMU-like component in the mantle source. Besides low $^{87}Sr/^{86}Sr_i$ (<0.7031) and high $^{143}Nd/^{144}Nd_i$ (>0.5128) ratios, this lava is characterized by radiogenic Pb isotope compositions ($^{206}Pb/^{204}Pb > 19.3$, $^{207}Pb/^{204}Pb > 15.6$, $^{208}Pb/^{204}Pb > 39.3$), suggesting an origin from a depleted mantle source with HIMU-like isotopic signature.

Based on the results discussed above, we propose that the Coyhaique basalt is similar to basalts in southernmost Patagonia (Choo et al., 2012;

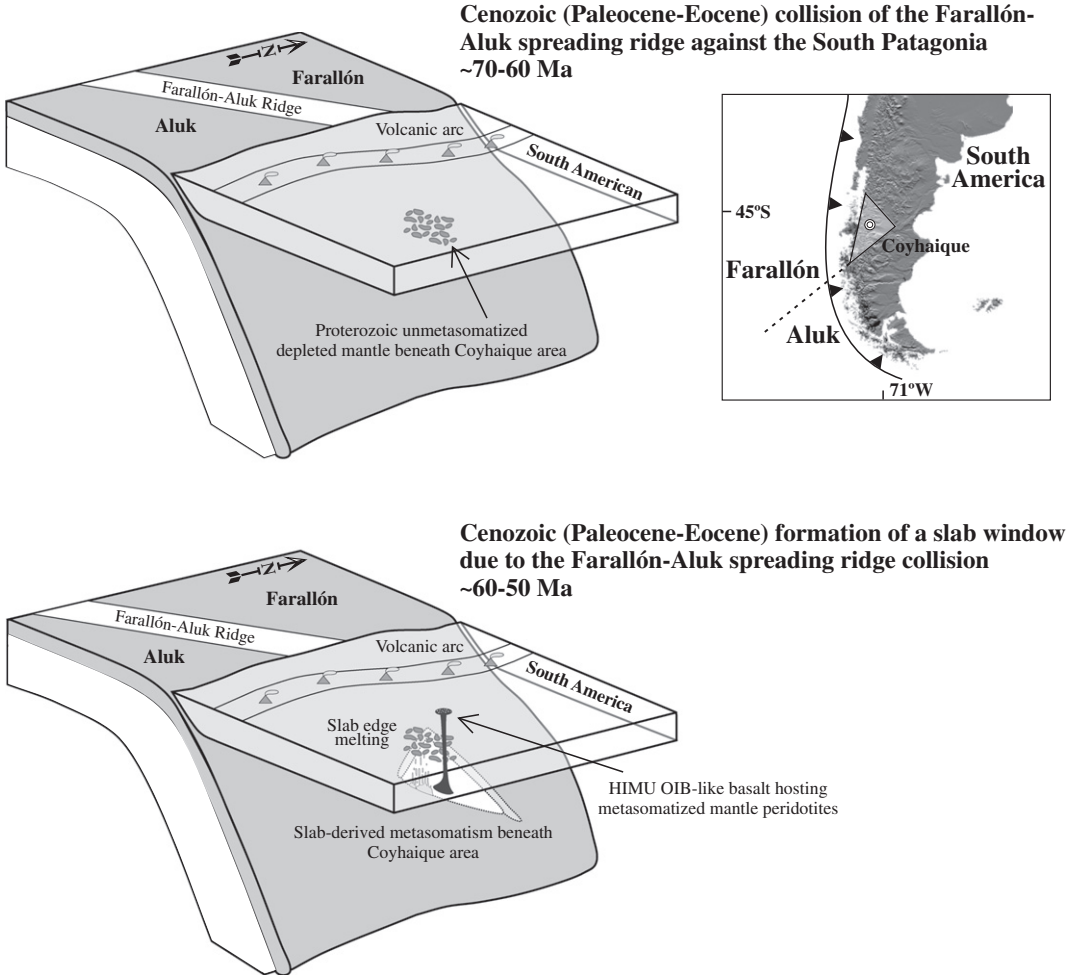

Fig. 12. Tectono-magmatic evolution of the upper mantle beneath the Coyhaique locality during Paleocene–Eocene time (70–50 Ma). The Farallón–Aluk ridge collision in southern South America resulted in a slab-free zone, or slab window, through which asthenospheric mantle can ascend. The Coyhaique lava likely record the upwelling of a deeper sub-slab asthenosphere beneath the Aysén Region. When this magma erupted, it carried Proterozoic mantle xenoliths to the surface. These xenoliths were metasomatized by slab melts released from a mixture of subducted sediments and oceanic crust during the initial stages of the Farallón–Aluk ridge collision in Paleocene–Eocene time or by an even older subduction-related event.

D'Orazio et al., 2000; Stern et al., 1990) and the Antarctic Peninsula (e.g., Hole, 1990; Hole et al., 1993), which are characterized by depleted HIMU-like OIB asthenospheric signatures and markedly different from the composition of the MORBs. Compared to typical HIMU lavas (e.g., Sta. Helena and the Cook-Austral Islands; Hanyu et al., 2014), the studied basalt shows significant low $^{206}Pb/^{204}Pb$, which suggests that the source region of Eocene Coyhaique lava could have been affected by an ancient (Mesozoic or earlier) subduction-related event. One possibility is that the subcontinental asthenospheric mantle was modified by processes associated with a prolonged period of subduction related to the Andean orogenesis and the recycling of several oceanic plates beneath the continent since the Mesozoic breakup of Gondwana, or by an even older subduction-related event.

6. Conclusions

The coarse- to medium-grained spinel-lherzolites hosted in the Eocene alkaline basalt at Coyhaique locality have protogranular to porphyroblastic textures, which indicate low strain and recrystallization rates. The depletion in SiO_2 and moderate enrichment in MgO compared to the PM and DMM compositions, as well as the negative correlations between MgO and the basaltic components (e.g., Al_2O_3, CaO and TiO_2), indicate that the Coyhaique spinel-lherzolites are solid SCLM residues derived from a common fertile source following variable degrees of partial melting (<8%). The majority of the spinel-lherzolites show flat PM-normalized REE patterns, but some samples show slight LREE depletion ($Ce/Yb_N = 0.6$) and others are LREE enriched ($Ce/Yb_N = 1.8$). Trace element compositions of the studied spinel-lherzolites show characteristics that are typical of arc magmas, such as pronounced negative Nb–Ta–Ti anomalies coupled with a significant enrichment of LILE (e.g., U) and chalcophile elements (W, Pb and Sn). Correlations among certain trace element ratios [e.g., (Th–Pb)/Ce, (Ba–U–Pb–Sr)/Th] and Sr–Nd–Pb isotopic ratios point to mixing of depleted mantle components (at least 90% of DMM or PREMA) with an enriched slab-derived component (up to 10%). According to our model, the slab-derived component in the depleted SCLM contains 50% subducted Chile Trench sediments and 50% modified oceanic crustal melts probably produced during the initial stages of the Farallón–Aluk ridge collision during Paleocene–Eocene time. However, we do not preclude the possibility that the metasomatism recorded by Coyhaique peridotites is related to an older subduction event. Conversely, there is no evidence that OIB-like asthenospheric melts transported through the Farallón–Aluk asthenospheric slab window metasomatized the depleted SCLM beneath the Coyhaique area.

The Eocene host alkaline basalt related to the Balmaceda Basalt unit has a HIMU-like OIB affinity, which is supported by marked positive Nb–Ta anomalies coupled with negative anomalies in highly incompatible and fluid-mobile elements (Rb, K, Pb, and Sr). The low $^{87}Sr/^{86}Sr_i$

(<0.70306) and relatively high $^{143}Nd/^{144}Nd_i$ (>0.51287) and $^{206}Pb/^{204}Pb$ (>19.3) isotopes are consistent with a HIMU-like OIB mantle source. This basalt was generated by small degrees of partial melting (up to 6%) that resulted from asthenospheric upwelling through the slab window related to the Farallón–Aluk ridge collision and subduction beneath south Patagonia during Eocene time. The Coyhaique basalt has low $^{206}Pb/^{204}Pb$ ratios compared to end-member HIMU lavas (e.g., Sta. Helena and the Cook–Austral Islands). This suggests that this region could have been modified by processes associated with a prolonged period of subduction related to the Andean orogenesis and the recycling of several oceanic plates beneath the continent since the Mesozoic breakup of Gondwana, or by an even older subduction-related event.

Acknowledgements

The National Council of Technological and Scientific Development – CNPq, Brazil, JSPS KAKENHI Grant Numbers 21403012 & 15H02630 awarded to Y. O. and the Earthquake Research Institute (ERI) cooperative research program, University of Tokyo, supported this study. We are thankful to N. Hokanishi for help with the XRF analysis and M. Assis, A. Martins, G. Raupp, and L. Carniel for assistance with the isotopic procedures. The authors are also grateful to A. Chapman and T. Riley for their constructive comments and suggestions on earlier versions of the manuscript. Finally, we thank A. Kerr for his comments and efficient editorial handling.

Appendix A

Table A.1
Trace element data with duplicate analysis of sample PM25-34 and a reference material (MRG-1).

			Precision			Accuracy
	Limit of Detection	Sample	Sample duplicate	Reference Material	Reference material original data from MUN	
		PM25-34	PM25-34	MRG-1 (run)	MRG-1 (MUN 495-633)	MRG-1 (run/MUN reference material)
Cs	0.014	0.053	0.054	0.649	0.600	1.082
Rb	1.670	2.278	1.892	15.590	7.650	2.038
Ba	0.190	9.235	7.844	53.345	47.500	1.123
W	0.003	0.525	0.055	1.023	0.300	3.409
Th	0.019	0.382	0.125	1.070	0.780	1.372
U	0.013	0.105	0.109	0.279	0.250	1.115
Nb	0.020	0.106	0.160	19.757	22.300	0.886
Ta	0.004	0.009	0.012	0.826	0.830	0.996
La	0.011	1.196	0.969	9.661	9.070	1.065
Ce	0.014	3.110	3.330	25.587	26.200	0.977
Pb	0.054	0.198	0.106	4.219	5.200	0.811
Pr	0.011	0.486	0.453	4.017	3.790	1.060
Sr	0.204	20.119	22.026	260.647	274.000	0.951
Nd	0.069	2.084	1.833	19.346	18.300	1.057
Sm	0.082	0.545	0.401	4.561	4.510	1.011
Zr	0.023	16.092	18.609	100.867	93.700	1.076
Hf	0.081	0.44	0.431	4.389	3.760	1.167
Eu	0.022	0.174	0.143	1.453	1.460	0.995
Sn	0.240	0.206	0.108	2.839	3.6	0.789
Ti	2.507	833.908	711.121	22,072	22,601	0.977
Gd	0.043	0.711	0.681	4.338	4.110	1.056
Tb	0.006	0.118	0.106	0.598	0.550	1.087
Dy	0.049	0.820	0.817	3.265	3.010	1.085
Y	0.010	4.739	4.465	13.198	11.600	1.138
Ho	0.008	0.183	0.184	0.571	0.510	1.119
Er	0.032	0.569	0.565	1.481	1.210	1.224
Tm	0.010	0.091	0.102	0.254	0.150	1.694
Yb	0.057	0.569	0.501	1.171	0.810	1.446
Lu	0.012	0.086	0.081	0.166	0.110	1.511

MUN = Memorial University.

Table A.2
Classification and modal mineralogies for the Coyhaique mantle xenoliths. The modal proportions of the minerals were determined by point-counting with 900–2800 points covering the entire area of the relatively large thin sections. Abbreviations: Ol = olivine; Opx = orthopyroxene; Cpx = clinopyroxene; Sp = spinel.

Lithology: Lherzolite									
Samples:	PM25-5	PM25-9	PM25-12	PM25-15	PM25-17	PM25-18	PM25-21	PM25-22	PM25-25
Modal composition (vol.%)									
% Ol	47.2	62.6	48.5	55.2	56.8	56.5	62.1	56.3	57.6
% Opx	29.6	23.3	30.2	24.0	25.1	23.3	16.2	25.9	26.0
% Cpx	19.9	10.1	18.6	17.2	15.7	15.8	19.1	15.7	12.9
% Sp	3.3	4.0	2.7	3.6	2.4	4.4	2.6	2.1	3.5

Lithology: Lherzolite								
Samples:	PM25-26	PM25-27	PM25-28	PM25-30	PM25-31	PM25-34	PM25-35	PM25-38
Modal composition (vol.%)								
% Ol	58.0	61.8	41.7	62.3	59.0	56.2	52.1	61.5
% Opx	25.2	17.8	38.7	21.7	21.9	26.1	29.4	21.1
% Cpx	15.1	16.3	16.9	12.4	15.7	14.7	14.7	13.5
% Sp	1.7	4.1	2.7	3.6	3.4	3.0	3.8	3.9

Table A.3
Representative SEM-EDS analyses of the mineral assemblage from the Coyhaique mantle xenoliths. Total iron reported as FeO and Mg-number = Mg/(Mg + Fe). Abbreviations: Ol = olivine; Opx = orthopyroxene; Cpx = clinopyroxene; Sp = spinel; Id = iddingsite; Cpx reaction = spongy texture.

Sample:	PM25-9	PM25-5	PM25-9	PM25-5	PM25-9	PM25-5
Mineral phase:	Ol	Opx	Cpx	Sp	Id	Cpx reaction
SiO_2	40.02	53.94	50.70	-	49.20	51.92
Al_2O_3	–	5.67	7.48	58.61	–	4.09
FeO	10.84	6.35	3.01	11.16	17.11	3.68
MgO	49.14	33.28	15.78	22.14	33.69	18.24
CaO	–	0.76	20.17	–	–	21.17
Na_2O	–	–	2.11	–	–	0.90
Cr_2O_3	–	–	0.74	8.09	–	–
Total	100.18	99.93	99.99	100.00	100.00	100.00
Mg-number	89.97	91.21	91.21	79.70	79.58	90.75

References

Bach, W., Erzinger, J., Dosso, L., Bollinger, C., Bougault, H., Etoubleau, J., Sauerwein, J., 1996. Unusually large Nb–Ta depletions in North Chile ridge basalts at 36°50′ to 38°56′S: major element, trace element, and isotopic data. Earth and Planetary Science Letters 142, 223–240.

Baker, P.E., Rea, W.J., Skarmeta, J., Caminos, R., Rex, D.C., 1981. Igneous history of the Andean Cordillera and Patagonian Plateau around latitude 46°S. Philosophical Transactions of the Royal Society of London 303, 105–149.

Bjerg, E.A., Ntaflos, Th., Thöni, M., Aliani, P., Labudia, C.H., 2009. Heterogeneous lithospheric mantle beneath northern Patagonia: evidence from Prahuaniyeu garnet- and spinel-peridotites. Journal of Petrology 50 (7), 1267–1298.

Boutonnet, E., Arnaud, N., Guivel, C., Lagabrielle, Y., Scalabrino, B., Espinoza, F., 2010. Subduction of the South Chile active spreading ridge: a 17 Ma to 3 Ma magmatic record in central Patagonia (western edge of Meseta del Lago Buenos Aires, Argentina). Journal of Volcanology and Geothermal Research 189, 319–339.

Breitsprecher, K., Thorkelson, D.J., 2009. Neogene kinematic history of Nazca–Antarctic–Phoenix slab windows beneath Patagonia and the Antarctic Peninsula. Tectonophysics 464, 10–20.

Butler, R.F., Hervé, F., Munizaga, F., Beck, M.E., Burmester, R.F., Oviedo, E., 1991. Paleomagnetism of the Patagonian Plateau basalts, southern Chile and Argentina. Journal of Geophysical Research 96, 6023–6034.

Cande, S.C., Leslie, R.B., 1986. Late Cenozoic Tectonic of the Southern Chile trench. Journal of Geophysical Research 91, 471–496.

Castillo, P.R., 2006. An overview of adakite petrogenesis. Chinese Science Bulletin 51 (3), 257–268.

Cawood, P.A., Buchan, C., 2007. Linking accretionary orogenesis with supercontinent assembly. Earth-Science Reviews 82, 217–256.

Charrier, R., Linares, E., Niemeyer, H., Skármeta, J., 1979. K–Ar ages of basalt flows of Meseta Buenos Aires in southern Chile and their relation to the southeast Pacific triple junction. Geology 7, 436–439.

Chauvel, C., Dia, A.N., Bulurde, M., Chabaux, F., Durand, S., Ildefonse, P., Gerard, M., Deruelle, B., Ngounouno, I., 2005. Do decades of tropical rainfall affect the chemical compositions of basaltic lava flows in Mount Cameroon? Journal of Volcanology and Geothermal Research 141, 195–223.

Choo, M.K., Lee, M.J., Lee, J.I., Kim, K.H., Park, K.-H., 2012. Geochemistry and Sr–Nd–Pb isotopic constraints on the petrogenesis of Cenozoic lavas from the Pali Aike and Morro Chico area (52°S), southern Patagonia, South America. Island Arc 21, 327–350.

Demant, A., Hervé, F., Pankhurst, R.J., Suárez, M., 1996. Geochemistry of Early Tertiary back-arc basalts from Aysén, Southern Chile (44–46°S): geodynamic implications. Third International Symposium on Andean Geodynamics, No. 3, Actas, pp. 555–558 (St. Malo, France).

Diegor, W., Longerich, H., Abrajano, T., Horn, I., 2001. Applicability of a high pressure digestion technique to the analysis of sediment and soil samples by inductively coupled plasma-mass spectrometry. Analytica Chimica Acta 431, 195–207.

Domeier, M., Torsvik, T.H., 2014. Plate tectonics in the late Paleozoic. Geoscience Frontiers 5, 303–350.

D'Orazio, M., Agostini, S., Mazzarini, F., Innocenti, F., Manetti, P., Haller, M., Lahsen, A., 2000. The Pali Aike Volcanic Field, Patagonia: slab-window magmatism near the tip of South America. Tectonophysics 321, 407–427.

Espinoza, F., Morata, D., Pelleter, E., Maury, R.C., Suárez, M., Lagabrielle, Y., Polvé, M., Bellon, H., Cotten, J., De la Cruz, R., Guivel, C., 2005. Petrogenesis of the Eocene and Mio–Pliocene alkaline basaltic magmatism in Meseta Chile Chico, southern Patagonia, Chile: evidence for the participation of two slab windows. Lithos 82, 315–343.

Faccini, B., Bonadiman, C., Coltorti, M., Grégoire, M., Siena, F., 2013. Oceanic material recycled within the Sub-Patagonian Lithospheric Mantle (Cerro del Fraile, Argentina). Journal of Petrology 54, 1211–1258.

Fitton, J.G., Saunders, A.D., Norry, M.J., Hardarson, B.S., Taylor, R.N., 1997. Thermal and chemical structure of the Iceland plume. Earth and Planetary Science Letters 153, 197–208.

Gervasoni, F., Conceição, R.V., Jalowitzki, T.L.R., Schilling, M.E., Orihashi, Y., Nakai, S., Sylvester, P., 2012. Heterogeneidades do manto litosférico subcontinental no extremo sul da Placa Sul-americana: influência da subducção atual e interações litosfera-astenosfera sob o Campo Vulcânico de Pali Aike. Pesquisas em Geociências 39, 269–285.

Gervasoni, F., Klemme, S., Rohrbach, A., Grützner, T., Berndt, J., 2017. Experimental constraints on mantle metasomatism caused by silicate and carbonate melts. Lithos 282-283, 173–186.

Gorring, M.L., Kay, S.M., 2000. Carbonatite metasomatized peridotite xenoliths from southern Patagonia: implications for lithospheric processes and Neogene plateau magmatism. Contributions to Mineralogy and Petrology 140, 55–72.

Gorring, M.L., Singer, B., Gowers, J., Kay, S.M., 2003. Plio-Pleistocene basalts from the Meseta del Lago Buenos Aires, Argentina: evidence for asthenosphere–lithosphere interactions during slab window magmatism. Chemical Geology 193, 215–235.

Hanyu, T., Kawabata, H., Tatsumi, Y., Kimura, J.-I., Hyodo, H., Sato, K., Miyazaki, T., Chang, Q., Hirahara, Y., Takahashi, T., Senda, R., Nakai, S., 2014. Isotope evolution in the HIMU reservoir beneath St. Helena: implications for the mantle recycling of U and Th. Geochimica et Cosmochimica Acta 143, 232–252.

Hauff, F., Hoernle, K., Schmidt, A., 2003. Sr–Nd–Pb composition of Mesozoic Pacific oceanic crust (Site 1149 and 801, ODP Leg 185): implications for alteration of ocean crust and the input into the Izu–Bonin–Mariana subduction system. Geochemistry, Geophysics, Geosystems 4, 1–30.

Hawkesworth, C.J., Turner, S.P., McDermott, F., Peate, D.W., van Calsteren, P., 1997. U–Th isotopes in arc magmas: implications for element transfer from the subducted crust. Science 276, 551–555.

Hervé, F., Pankhurst, R.J., Fanning, C.M., Calderón, M., Yaxley, G.M., 2007. The South Patagonian batholith: 150 my of granite magmatism on a plate margin. Lithos 97, 373–394.

Hickey, R.L., Frey, F.A., Gerlach, D.C., 1986. Multiple sources for basaltic arc rocks from the southern volcanic zone of the Andes (34°−41°S): trace element and isotopic evidence for contributions from subducted oceanic crust, mantle, and continental crust. Journal of Geophysical Research 91, 5963–5983.

Hickey-Vargas, R., Moreno-Roa, H., López-Escobar, L., Frey, F.A., 1989. Geochemical variations in Andean basaltic and silicic lavas from the Villarrica–Lanin volcanic chain (39.5°S): an evaluation of source heterogeneity, fractional crystallization and crustal assimilation. Contributions to Mineralogy and Petrology 103, 361–386.

Hole, M.J., 1990. Geochemical evolution of Pliocene-recent post-subduction alkalic basalts from Seal Nunataks, Antarctic Peninsula. Journal of Volcanology and Geothermal Research 40, 149–167.

Hole, M.J., Kempton, P.D., Millar, I.L., 1993. Trace element and isotopic characteristics of small-degree melts of the asthenosphere: evidence from the alkalic basalts of the Antarctic Peninsula. Chemical Geology 109, 51–68.

Ionov, D.A., Ashchepkov, I., Jagoutz, E., 2005. The provenance of fertile off-craton lithospheric mantle: Sr–Nd isotope and chemical composition of garnet and spinel peridotite xenoliths from Vitim, Siberia. Chemical Geology 217, 41–75.

Jacques, G., Hoernle, K., Gill, J., Hauff, F., Wehrmann, H., Garbe-Schönberg, D., van den Bogaard, P., Bindeman, I., Lara, L.E., 2013. Across-arc geochemical variations in the Southern Volcanic Zone, Chile (34.5–38.0°S): constraints on mantle wedge and slab input compositions. Geochimica et Cosmochimica Acta 123, 218–243.

Jalowitzki, T., Conceição, R.V., Orihashi, Y., Bertotto, G.W., Nakai, S., Schilling, M.E., 2010. Evolução geoquímica de peridotitos e piroxenitos do manto litosférico subcontinental do vulcão Agua Poca, Terreno Cuyania, Argentina. Pesquisas em Geociências 37 (2), 143–167.

Jalowitzki, T., Sumino, S., Conceição, R.V., Orihashi, Y., Nagao, K., Bertotto, G.W., Balbinot, E., Schilling, M.E., Gervasoni, F., 2016. Noble gas composition of subcontinental lithospheric mantle: an extensively degassed reservoir beneath Southern Patagonia. Earth and Planetary Science Letters 450, 263–273.

Jenner, G.A., Longerich, H.P., Jackson, S.E., Fryer, B.J., 1990. ICP-MS - a powerful tool for high-precision trace-element analysis in earth sciences: evidence from analysis of selected U.S.G.S. reference samples. Chemical Geology 83, 133–148.

Johnson, K.T.M., 1998. Experimental determination of partition coeffcients for rare earth and high-field-strength elements between clinopyroxene, garnet, and basaltic melt at high pressures. Contributions to Mineralogy and Petrology 133, 60–68.

Karsten, J.L., Klein, E.M., Sherman, S.B., 1996. Subduction zone geochemical characteristics in ocean ridge basalts from the southern Chile Ridge: implications of modem ridge subduction systems for the Archean. Lithos 37, 143–161.

Kay, S.M., Ramos, V.A., Marquez, M., 1993. Evidence in Cerro Pampa volcanic rocks for slab-melting prior to ridge-trench collision in Southern South America. The Journal of Geology 101, 703–714.

Kay, S.M., Ramos, V.R., Gorring, M.L., 2002. Geochemistry of Eocene plateau basalts related to ridge collision in Southern Patagonian. XV Congreso Geológico Argentino. Actas 3, pp. 60–65.

Kilian, R., Behrmann, J.H., 2003. Geochemical constraints on the sources of Southern Chile Trench sediments and their recycling in arc magmas of the Southern Andes. Journal of the Geological Society 160, 57–70.

Kilian, R., Stern, C.R., 2002. Constraints on the interaction between slab melts and the mantle wedge from adakitic glass in peridote xenoliths. European Journal of Mineralogy 14, 25–36.
Labanieh, S., Chauvel, C., Germa, A., Quidelleur, X., 2012. Martinique: a clear case for sediment melting and slab dehydration as a function of distance to the trench. Journal of Petrology 53 (12), 2441–2464.
Lloyd, G.E., Farmer, A.B., Mainprice, D., 1997. Misorientation analysis and the formation and orientation of subgrain and grain boundaries. Tectonophysics 279, 55–78.
Lucassen, F., Wiedicke, M., Franz, G., 2010. Complete recycling of a magmatic arc: evidence from chemical and isotopic composition of Quaternary trench sediments in Chile (36°–40°S). International Journal of Earth Sciences 99, 687–701.
McDonough, W.F., 1990. Constraints on the composition of the continental lithospheric mantle. Earth and Planetary Science Letters 101, 1–18.
McDonough, W.F., Sun, S.-S., 1995. Composition of the Earth. Chemical Geology 120, 223–253.
Mercier, J.C., Nicolas, A., 1975. Textures and fabrics of upper-mantle peridotites as illustrated by xenoliths from basalt. Journal of Petrology 16, 454–487.
Morata, D., de la Cruz, R., Suárez, M., Demant, A., 2000. Mantle xenoliths and xenocrysths in the late Paleocene Patagonian continental flood basalts from Aysen, S. Chile. IX Congreso Geologico Chileno. Actas 2, pp. 226–229.
Moyen, J.-F., 2009. High Sr/Y and La/Yb ratios: the meaning of the "adakitic signature". Lithos 112, 556–574.
Mundl, A., Ntaflos, T., Ackerman, L., Bizimis, M., Bjerg, E.A., Hauzenberger, C.A., 2015. Mesoproterozoic and Paleoproterozoic subcontinental lithospheric mantle domains beneath southern Patagonia: isotopic evidence for its connection to Africa and Antarctica. Geology 43, 39–42.
Nagao, K., Ogata, A., Miura, Y., Matsuda, J., Akimoto, S., 1991. Highly reproducible 13 and 17 ka K–Ar ages of two volcanic rocks. Geochemical Journal 25, 447–451.
Niu, Y., Hékinian, R., 1997. Basaltic liquids and harzburgitic residues in the Garrett Transform: a case study at fast-spreading ridges. Earth and Planetary Science Letters 146, 243–258.
Ntaflos, Th., Bjerg, E.A., Labudia, C.H., Kurat, G., 2007. Depleted lithosphere from the mantle wedge beneath Tres Lagos, southern Patagonia, Argentina. Lithos 94, 46–65.
Orihashi, Y., Hirata, T., 2003. Rapid quantitative analysis of Y and REE abundances in XRF glass bead for selected GSJ reference rock standards using UV laser ablation ICP-MS. Geochemical Journal 37, 401–412.
Orihashi, Y., Naranjo, J.A., Motoki, A., Sumino, H., Hirata, D., Anma, R., Nagao, K., 2004. Quaternary volcanic activity of Hudson and Lautaro volcanoes, Chilean Patagonia: new constraints from K–Ar ages. Andean Geology 31, 207–224.
Orihashi, Y., Anma, R., Motoki, A., Haller, M.J., Hirata, D., Iwano, H., Sumino, H., Ramos, V.A., 2013. Evolution history of the crust underlying Cerro Pampa, Argentine Patagonia: constraint from LA–ICPMS U–Pb ages for exotic zircons in the Mid-Miocene adakite. Geochemical Journal 47, 235–247.
Pankhurst, R.J., Weaver, S.D., Hervé, F., Larrondo, P., 1999. Mesozoic–Cenozoic evolution of the North Patagonian Batholith in Aysén, southern Chile. Journal of the Geological Society of London 156, 673–694.
Parada, M.A., Lahsen, A., Palacios, C., 2001. Ages and geochemistry of Mesozoic–Eocene back-arc volcanic rocks in the Aysén region of the Patagonian Andes, Chile. Revista Geológica de Chile 28 (1), 25–46.
Pearce, J.A., 2008. Geochemical fingerprinting of oceanic basalts with applications to ophiolite classification and the search for Archean oceanic crust. Lithos 100, 14–48.
Ramos, V.A., Kay, S.M., 1992. Southern Patagonian plateau basalts and deformation: back-arc testimony of ridge collisions. Tectonophysics 205, 261–282.
Rieck Jr., N., Conceição, R.V., Koester, E., Dantas, C., 2007. O manto litosférico continental na região do Cerro de Los Chenques, Argentina: Evidências de heterogeneidade e metassomatismo. Geologia USP Série Científica 7 (1), 1–17.
Rivalenti, G., Mazzucchelli, M., Laurora, A., Ciuffi, S.I.A., Zanetti, A., Vannucci, R., Cingolani, C.A., 2004. The backarc mantle lithosphere in Patagonia, South America. Journal of South American Earth Sciences 17, 121–152.
Salters, V.J.M., Sachi-Kocher, A., 2010. An ancient metasomatic source for the Walvis Ridge basalts. Chemical Geology 273, 151–167.
Schilling, M., Conceição, R.V., Mallmann, G., Koester, E., Kawashita, K., Hervé, F., Morata, D., Motoki, A., 2005. Spinel-facies mantle xenoliths from Cerro Redondo, Argentine Patagonia: petrographic, geochemical, and isotopic evidence of interaction between xenoliths and host basalt. Lithos 82, 485–502.
Schilling, M.E., Carlson, R.W., Tassara, A., Conceição, R.V., Bertotto, G.W., Vásquez, M., Muñoz, D., Jalowitzki, T., Gervasoni, F., Morata, D., 2017. The origin of Patagonia revealed by Re–Os systematics of mantle xenoliths. Precambrian Research 294, 15–32.
Shaw, D.M., 2006. Trace Elements in Magmas: A Theoretical Treatment. Cambridge University Press (256 pp.).
Shinjoe, H., Orihashi, Y., Naranjo, J.A., Hirata, D., Hasenaka, T., Fukuoka, T., Sano, T., Anma, R., 2013. Boron and other trace element constraints on the slab-derived component in Quaternary volcanic rocks from the Southern Volcanic Zone of the Andes. Geochemical Journal 47, 185–199.
Staudigel, H., Plank, T., White, B., Schminck, H.-U., 1996. Geochemical Fluxes During Seafloor Alteration of the Basaltic Upper Oceanic Crust: DSDP Sites 417 and 418. In: Bebout, G.E., Scholl, D.W., Kirby, S.H., Platt, J.P. (Eds.), Subduction Top to Bottom. Geophysical Monograph 96. American Geophysical Union, Washington, D.C., pp. 19–38.
Stern, C.R., Kilian, R., 1996. Role of the subducted slab, mantle wedge and continental crust in the generation of adakites from the Andean Austral Volcanic Zone. Contributions to Mineralogy and Petrology 123, 263–281.
Stern, C.R., Frey, F.A., Futa, K., Zartman, R.E., Peng, Z., Kyser, T.K., 1990. Trace element and Sr, Nd, Pb, and O isotopic composition of Pliocene and Quaternary alkali basalts of the Patagonian plateau lavas of southernmost South America. Contributions to Mineralogy and Petrology 104, 294–308.
Stern, C.R., Kilian, R., Olker, B., Hauri, E.H., Kyser, T.K., 1999. Evidence from mantle xenoliths for relatively thin (<100 km) continental lithosphere below the Phanerozoic crust of southernmost South America. Lithos 48, 217–235.
Streckeisen, A., 1979. Classification and nomenclature of volcanic rocks, lamprophyres, carbonatites, and melilitic rocks: recommendations and suggestions of the IUGS subcommission on the systematics of igneous rocks. Geology 7, 331–335.
Sturm, M.E., Klein, E.M., Graham, D.W., Karsten, J., 1999. Age constraints on crustal recycling to the mantle beneath the southern Chile Ridge: He–Pb–Sr–Nd isotope systematics. Journal of Geophysical Research 104, 5097–5114.
Sun, S., McDonough, W.F., 1989. Chemical and isotopic systematics of oceanic basalts, implications for mantle composition and processes. In: Saunders, A.D., Norry, M.J. (Eds.), Magmatism in the Ocean Basins. Geological Society (Special Publications) 42, pp. 313–345.
Tani, K., Orihashi, Y., Nakada, S., 2002. Major and trace component analysis of silicate rocks using fused glass bead by X-ray fluorescence spectrometer: evaluation of analytical precision for third, sixth and eleventh dilution fused glass beads. Tech. Res. Rep. 8. ERI, Univ. Tokyo, pp. 26–36
Weaver, B.L., 1991. The origin of ocean island basalts end-member compositions: trace element and isotopic constraints. Earth and Planetary Science Letters 104, 381–397.
Workman, R.K., Hart, S.R., 2005. Major and trace element composition of the depleted MORB mantle (DMM). Earth and Planetary Science Letters 231, 53–72.
Workman, R.K., Hart, S.R., Jackson, M., Regelous, M., Farley, K.A., Blusztajn, J., Kurz, M., Staudigel, H., 2004. Recycled metasomatized lithosphere as the origin of the enriched mantle II (EM-2) end-member: evidence from the Samoan volcanic chain. Geochemistry, Geophysics, Geosystems 5, 1–44.
Wörner, G., Zindler, A., Staudigel, H., Schmincke, H.U., 1986. Sr, Nd, and Pb isotope geochemistry of Tertiary and Quaternary alkaline volcanics from West Germany. Earth and Planetary Science Letters 79, 107–119.